Research Square

Preprints are preliminary reports that have not undergone peer review.
They should not be considered conclusive, used to inform clinical practice,
or referenced by the media as validated information.

Bipolar Cell Targeted Optogenetic Gene Therapy Restores Parallel Retinal Signaling And High-Level Vision In The Degenerated Retina

Jakub Kralik
University of Bern https://orcid.org/0000-0001-5216-9818
Michiel van Wyk
University of Bern
Nino Stocker
University of Bern
Sonja Kleinlogel (sonja.kleinlogel@unibe.ch)
University of Bern https://orcid.org/0000-0001-8272-7833

Article

Keywords: Optogenetic gene therapy, vision restoration, Opto-GPCRs, retina, retinal degeneration, patch-clamp, optomotor reflex, multi-electrode array recordings, visual cortex, rd1 mouse line

Posted Date: February 2nd, 2022

DOI: https://doi.org/10.21203/rs.3.rs-999738/v1

License: This work is licensed under a Creative Commons Attribution 4.0 International License.
Read Full License

Version of Record: A version of this preprint was published at Communications Biology on October 20th, 2022. See the published version at https://doi.org/10.1038/s42003-022-04016-1.

Bipolar cell targeted optogenetic gene therapy restores parallel retinal signaling and high-level vision in the degenerated retina

Jakub Kralik†, Michiel van Wyk†, Nino Stocker# and Sonja Kleinlogel*

Institute of Physiology and Department for BioMedical Research (DBMR), University of Bern, Switzerland
† Equal contribution.
# current address: Swiss Institute of Allergy and Asthma Research (SIAF), Davos, Switzerland
* Correspondence: sonja.kleinlogel@unibe.ch; Tel.: +41-(0)31-631-8705

Abstract: Optogenetic gene therapies to restore vision are in clinical trials. Whilst current clinical approaches target the ganglion cells, the output neurons of the retina, new molecular tools enable efficient targeting of the first order retinal interneurons, the bipolar cells, with the potential to restore a higher quality of vision. Here we investigate retinal signaling and behavioral vision in blind mice treated with bipolar cell targeted optogenetic gene therapies. All tested tools, including medium-wave opsin, Opto-mGluR6 and two new melanopsin based chimeras restored visual acuity and contrast sensitivity. The best performing opsin was a novel melanopsin-mGluR6 chimera, which in some cases restored visual acuities and contrast sensitivities that match wild-type animals. Light responses from the ganglion cells were robust with diverse receptive-field types, inferring elaborate inner retinal signaling. Our results highlight the potential of bipolar cell targeted optogenetics to recover high-level vision in human patients with end-stage retinal degenerations.

Keywords: optogenetic gene therapy; vision restoration; Opto-GPCRs; retina; retinal degeneration; patch-clamp; optomotor reflex; multi-electrode array recordings; visual cortex; *rd1* mouse line

1. Introduction

Optogenetic vision restoration has progressed rapidly to clinical trials. As opposed to other tissues, the retina is naturally accessible to light and the eye is immune-privileged, reducing the risk of adverse effects. In contrast to replacement gene therapies, optogenetics is a mutation-independent one-for-all therapy for photoreceptor degenerative diseases that creates replacement photoreceptors out of remaining inner retinal cells. The sole prerequisite is surviving inner retinal neurons. It was shown that the inner retina, in particular the bipolar cells, remain intact for years after photoreceptor loss [1] and seminal optogenetic restoration studies have demonstrated their functional integrity [2-5].

Current optogenetic trials (ClinicalTrials.gov Identifier: NCT03326336, NCT02556736, NCT04278131) introduce channelrhodopsin (ChR) variants to the retinal ganglion cells (RGCs), the output neurons of the retina, turning them into direct light detectors. However, a significant amount of image processing is performed presynaptic to the RGCs, by the bipolar and amacrine cell networks. The inner retinal circuitry dissects the visual scene into ~30 parallel channels that encode, for example, luminance, local contrast and directed movement [6]. This parallel processing of visual information is by-passed when directly imparting light sensitivity to the RGCs.

As photoreceptors degenerate, the bipolar cells, which normally receive input from the photoreceptors, become the first surviving cells within the retinal hierarchy. Direct optogenetic stimulation of bipolar cells therefore preserves inner retinal processing, and with that, diverse RGC receptive-fields, which has the potential to restore higher quality vision compared to RGC targeted approaches.

Recently developed synthetic AAVs and ON-bipolar cell (OBC) specific promoters have paved the way for OBC-targeted optogenetic vision restoration [7]. To date, both native and engineered opsins have been expressed in OBCs to successfully restore retinal light responses [2-5,7,8]. When ectopically expressed in OBCs, these opsins trigger the Gαo signaling cascade of the primary OBC receptor, the metabotropic glutamate receptor 6 (mGluR6). mGluR6 is exclusively expressed in the postsynaptic region of OBCs [9] and signals via the Gαo G-protein pathway [10] to gate transient receptor potential melastatin 1 (TRPM1) non-selective cation channels [11,12]. A key advantage of this approach is that signal amplification inherent to metabotropic receptors make GPCR opsins approximately 1000-fold more light sensitive compared to ChRs. Rhodopsin [2] and medium-wave cone opsin (OPN1MW) [4,7] have both been successfully expressed in

OBCs to restore vision. Both these opsins naturally activate Gt (transducin) in photoreceptors, but also activate Gαo, which belongs to the same G-protein family. In an attempt to optimize activation of the OBC's Gαo signaling pathway, we have previously engineered a chimera of melanopsin with the intracellular domains exchanged by those of mGluR6 (Opto-mGluR6). This successfully converted the Gαq-protein tropism of melanopsin to the Gαo tropism of mGluR6 [5].

Here we elucidate the full potential of OBC-targeted Opto-GPCRs in vision restoration. We functionally compare Opto-mGluR6 [5], OPN1MW-mGluR6 [7] and two new melanopsin-mGluR6 chimeras. We show that all opsins are functional and able to restore vision at the retinal, cortical and behavioral levels. The C-terminus of mGluR6 enhanced functional opsin expression. Signaling in the RGC population was diverse with ON and OFF as well as transient and sustained visual cannels and had the capacity to adapt to environmental light intensities. Pathophysiological changes associated with retinal degeneration introduced some "sluggishness" to restored RGC light responses. Nonetheless, we show that an OBC-targeted optogenetic therapy has the potential to restore visual acuities and contrast sensitivities in blind *rd1* mice close to wild-type values. On the background of a recent report of successful object localization by a patient treated with the ChR variant ChrimsonR targeted at the macular RGCs [13], the encouraging results of this study anticipate that a higher quality vision can be restored in human patients through OBC-targeted optogenetic gene therapies.

2. Results

2.1. Screening of opsin constructs in HEK293-GIRK cells

GPCR opsins previously used in OBC-targeted gene therapies include the Opto-mGluR6 chimera[5], rhodopsin[2], medium-wave cone opsin (OPN1MW)[4,7] and lamprey parapinopsin[14]. Our aim was to examine the maximum potential of this therapeutic approach. In light of potential clinical use we initially focused on human OPN1MW (a canonical bleachable ciliary pigment) and human melanopsin (a bleach resistant tri-stable opsin)[15]. We tested Opto-mGluR6[5], two additional melanopsin-mGluR6 chimeras, Mela(CTmGluR6) and Mela(CT+IL3mGluR6), and OPN1MW(CTmGluR6)[7]. In Mela(CTmGluR6) and in OPN1MW(CTmGluR6), we replaced the native opsin carboxyl termini by that of mGluR6, the resident receptor in OBCs that is naturally activated by glutamate released from the photoreceptors[16]. This was done to accelerate the kinetics of melanopsin[17,18] and to support subcellular trafficking in the target OBCs[5]. Mela(CT+IL3mGluR6) has, in addition, the intracellular loop 3 (IL3) of melanopsin replaced by that of mGluR6, a region known to be important for G-protein selectivity[19]. Mela(CT+IL3mGluR6) was not straightforward to design, since IL3 is particularly long in melanopsin but very short in mGluR6. Unlike the initial design of Opto-mGluR6 where the entire IL3 of melanopsin was replaced, we here opted for a strategy where the relatively short IL3 of mGluR6 replaced only part of melanopsin's IL3.

We first tested expression and function of all chimeric constructs in HEK293-GIRK cells, which stably express the Kir3.1/Kir3.2 potassium channel opened by Gβγ G-protein subunits released by activated G-proteins of the Gαi/o family. Since the TRPM1 channels driving excitation in OBCs are also Gβγ-gated [20], GIRK channel coupling presents a relevant *in vitro* functional assay for the target mGluR6 pathway in OBCs. While functional recordings were made using opsin-IRES-TurboFP635 constructs, we also fused all opsin chimeras directly to the fluorescent protein mKate2 to monitor membrane localization. All proteins targeted well to the cell membrane and expression extended into the fine filipods (Fig. 1A). All four opsin constructs activated GIRK currents in response to 470nm light (10^{14} photons/cm^2/s, Figs. 1B&C). Currents elicited by Opto-mGluR6 were significantly smaller (3.9 ± 1.8 pA/pF, n = 4; mean ± SEM) than those elicited by the other constructs ($p < 0.0001$). This may be due to the extensive chimeric design, which may reduce the efficacy of the engineered Opto-mGluR6. Alternatively, Opto-mGluR6's tropism may be almost completely shifted towards Gαo, which is not expressed in HEK293 cells[21], whereas parent OPN1MW and melanopsin are able to activate the Gαi-type G-proteins endogenously expressed in the HEK293-GIRK cell line. Similar effects could explain reduced GIRK currents elicited by Mela(CT+IL3mGluR6) (44.0 ± 3.7pA/pF, n = 5, mean ± SEM), which were significantly smaller compared to those elicited by Mela(CTmGluR6) (98.0 ± 9.7pA/pF, n = 5, mean ± SEM; $p = 0.002$). Notably, the mGluR6 C-terminus significantly increased GIRK-current densities in OPN1MW [OPN1MW(CTmGluR6): 78.0 ± 9.6pA/pF, mean ± SEM, n = 14; OPN1MW: 46.1 ± 7.8pA/pF, n = 13; $p = 0.027$] and in melanopsin [WT melanopsin: 22.0 ± 5.7pA/pF, n = 5; $p = 0.0005$ compared to Mela(CTmGluR6)], inferring that the mGluR6 C-terminus enhances expression of activatable opsin. All constructs activated GIRK currents with similar ON kinetics [Fig. 1D; Mela(CTmGluR6): 0.7 ± 0.2s, n=5; Mela(CT+IL3mGluR6): 1.6 ± 0.3s, n=5; OPN1MW(CTmGluR6): 0.8 ± 0.2s, n=6] and OFF kinetics [Fig. 1E; Mela(CTmGluR6): 12.1 ± 2.3s; n=6; Mela(CT+IL3mGluR6): 12.8 ± 1.7s, n=5; OPN1MW(CTmGluR6): 9.8 ± 2.2s, n=6], providing evidence that melanopsin, without its regulatory C-terminus, is not inherently slow.

Next, we compared the relative bleach stabilities of Mela(CTmGluR6) and OPN1MW(CTmGluR6), an imperative property when considering a role in vision restoration. In particular, photoreceptor degeneration is often associated with pathologies of the retinal pigment epithelium resulting in a compromised visual cycle and a restricted supply of cis retinal, which may impact the function of monostable opsins such as OPN1MW. Melanopsin, a tri-stable pigment, is able to recycle its chromophore, a property shared by many invertebrate and microbial relatives (i.e. ChR2) that imparts bleach resistance. To demonstrate this difference between OPN1MW and melanopsin chimeras, we presented cells with consecutive light flashes (470nm; 5 x 10^{13} photons/cm^2/s) without providing 9-cis retinal. As expected, cells expressing OPN1MW(CTmGluR6) had a rapid response rundown compared to Mela(CTmGluR6) (Fig. 1F). When stimulated with an orange backlight (595 nm; 5 x 10^{15} photons/cm^2/s), cells expressing Mela(CTmGluR6) retained full response amplitude, even at high light stimulation frequencies (0.2 Hz; Fig. 1G). The backlight also accelerated the OFF-kinetics of Mela(CTmGluR6) (2.9 ± 0.3s; n=6; p = 0.0008, Fig. 1E, Suppl. Fig. S1) to values significantly faster than those of monostable OPN1MW(CTmGluR6) (p=0.007), a further advantage of using a bi-stable optogenetic tool.

2.2. Functional screening by the optomoter reflex (OMR)

We have previously established automated optomotor reflex (OMR) screening as a fast and reliable *in vivo* readout for optogenetically restored visual function[5,7]. The OMR is based on the vestibulo–ocular reflex that evokes head movements to stabilize an image on the retina and is driven mainly by ON-direction-selective ganglion cells (ON-DSGCs)[22]. We tested the performance of all four opsin constructs in restoring naïve behavioral OMR responses when expressed in the OBCs of the degenerated *rd1* mouse retina. Although the OBC population, particularly in the degenerated retina, was proven difficult to transfect[23], recent molecular advances, such as synthetic AAV capsids and cell-specific short promoters now enable efficient and selective OBC targeting *in vivo*[7]. We packaged all opsin construct in the AAV2.7m8 vector[24] under control of the 770En_454P(h*GRM6*) promoter[7]. We injected blind *rd1* mice bilaterally and intravitreally with titer-matched vectors (10^{10} vg/eye) and assessed restored visual function at >24 weeks of age when photoreceptors and light-responses have completely disappeared in untreated *rd1* littermates[25]. By determining the spatial frequency or contrast thresholds at which drifting sinusoidal gratings trigger head movements, we inferred both, the visual acuity and contrast sensitivity of the OMR[26].

Figure 1H summarizes the visual acuity thresholds reached by the different treatment groups and relates them to average values achieved by sighted C57BL/6J mice (0.44 ± 0.063 cyc/deg, n=10) and untreated *rd1* littermates (0.03 ± 0.03 cyc/deg, n=15). All four opsin constructs significantly restored visual acuity in treated *rd1* mice. Mela(CTmGluR6) (0.37 ± 07 cyc/deg, n=16) significantly outperformed all other variants, including Mela(CT+IL3mGluR6) (0.18 ± 05 cyc/deg, n=5, p<0.001), OPN1MW(CTmGluR6) (0.21 ± 0.05 cyc/deg, n=5, p<0.001) and Opto-mGluR6 (0.27 ± 0.04 cyc/deg, n=12, p<0.001).

We next determined contrast sensitivity thresholds by decreasing the luminance levels between the stripes at the most sensitive spatial frequency of our treated *rd1* mice (0.125 cyc/deg, Suppl Fig. S2). Untreated *rd1* mice were unable to perform this task and were therefore excluded from the analysis and the graph shown in figure 1I. Mela(CTmGluR6) (4.5 ± 0.8 % Michelson contrast, n=11, mean ± s.e.m.) significantly outperformed Mela(CT+IL3mGluR6) (62.4 ± 8.6 % Michelson contrast, n=5, p < 0.001) and OPN1MW(CTmGluR6) (32.0 ± 5.8 % Michelson contrast, n=5, p=0001) treated *rd1* mice, but not Opto-mGluR6 treated mice (9.0 ± 3.5 % Michelson contrast, n=10, p=0.246). Remarkably, the contrast sensitivities restored by Mela(CTmGluR6) were not significantly different to those of normal sighted C57BL/6 mice (2.1 ± 0.4 % Michelson contrast, n=7, p=0.128).

Notably, the visual acuity and contrast sensitivity thresholds did not differ significantly in *rd1* mice that were tested at an older age (Suppl. Fig. S6) which is in line with previously reported long-term functional preservation of optogenetic gene therapies. These OMR data did not directly reflect the result of the HEK-GIRK screening. Opto-mGluR6 outperformed Mela(CT+IL3mGluR6) (p<0.05), whereas the performance of Mela(CT+IL3mGluR6) and OPN1MW(CTmGluR6) was not significantly different (p=0.999). This may reflect differences in the *in vivo* scenario, such as differences in protein expression or protein folding or differences in coupling to the Gαo (OBCs) and Gαi (HEK293 cells) G-protein subunit subtypes, as described above. Restored function also varied more in treated *rd1* mice compared to the controls, probably since the gene therapy typically leads to a heterogeneous expression pattern (Fig. 2A) with varying efficacy in different treated animals.

2.3. Mela(CTmGluR6) mediated light signaling in OBCs

The behavioral results indicate that light responses in the inner retina are restored. For more detailed investigations on the quality of retinal signaling, we selected Mela(CTmGluR6) since it restored vision with the highest sensitivity in the OMR.

Retinal explants from treated *rd1* mice showed pan-retinal expression of the optogenetic protein, albeit patchy in nature, with areas where almost all cells expressed and areas with much fewer expressing cells (Fig. 2A). Nevertheless, overall approximately half of OBCs in the *rd1* retina expressed Mela(CTmGluR6) (55.4 ± 11.6 %) and expression was selective for OBCs (64.9 ± 3.9%, Fig. 2B). These results were encouraging for late degenerated tissue that has undergone neuronal rewiring, gliosis and transcriptomic changes[27,28].

GPCR signaling is organized in subcellular domains with various intracellular interacting partners shaping the response[29,30]. To study the subcellular location of Mela(CTmGluR6), we expressed the Mela(CTmGluR6)-mKate fusion protein, which enabled direct observation of expression. In the wild-type retina, Mela(CTmGluR6)-mKate targeted to the dendrites and showed strong co-localization with Gαo, its primary interaction partner (Fig. 2C). We observed a similar expression pattern when expressing a mouse variant of Mela(CTmGluR6) that was visualized with an anti-mouse melanopsin antibody (Suppl. Fig. S3). In the degenerated *rd1* retina, Mela(CTmGluR6) trafficked predominantly to the cell bodies of the OBCs, as previously described for mGluR6 and the effector TRPM1 channel after the loss of photoreceptor input[31] (Suppl. Fig. S4). These immunohistochemical data confirm that Mela(CTmGluR6) is suitably located to couple into the endogenous mGluR6 signaling interactome in OBCs.

To functionally probe activation of the Gαo pathway within the OBCs, we performed cell-attached patch-clamp recordings from isolated OBCs and from OBCs in retinal whole mounts of *rd1* retinas. We targeted isolated OBCs from transduced C57BL/6 mice by their characteristic morphology under IR-DIC optics (Fig. 3A) and by fluorescent reporter expression (TurboFP635). The average membrane potential of isolated Mela(CTmGluR6)-expressing OBCs (-27.8 ± 1.8 mV, n=18) was not significantly different to that of non-transduced OBCs (-28.8 ± 2.7 mV, n=38; p=0.667), indicative that Mela(CTmGluR6) did not change the properties of OBCs. Only Mela(CTmGluR6)-expressing OBCs consistently responded with hyperpolarizations to a full-field blue light stimulus (1s duration, 470nm, 5 x 10^{14} photons/cm^2/s). Most OBCs responded with a relatively sustained response (presumably rod-type OBCs, Fig. 3B), whereas one cell, presumably a cone-type OBC, responded more transiently with very fast ON-kinetics (TauON: 90.0ms, TauOFF: 160.6ms, Fig. 3C). This suggests that diverse intrinsic processing of the Mela(CTmGluR6) signal introduces a segregation of response types already at the OBC level.

To investigate the temporal properties of OBC responses in a more relevant setting, we next recorded from OBCs in the whole mount preparation of fully degenerated *rd1* retinas where synaptic circuits (feed-back and feed-forward) remain intact (Fig. 3D). The OFF response kinetics of rod-type OBCs was significantly accelerated compared to the isolated configuration (Fig. 3E, TauOFF wholemount: 715 ± 350ms, n=9; TauOFF isolated: 1726 ± 985ms, n=11, p=0.0001), but no significant difference was found at the level of the ON kinetics (TauON wholemount: 339 ± 164 ms; TauON isolated: 383 ± 202m, p=0.303). Acceleration of the OFF kinetics agrees with the action of inhibitory amacrine cell feedback onto the OBC terminals in the whole mount situation. Confirming melanopsin's relative bleach resistance, responses could be triggered repeatedly at 0.4Hz in the absence of cis-retinal supplementation (Fig. 3F).

To compare Mela(CTmGluR6) and photoreceptor-mediated responses in OBCs, we also recorded from retinal slices of C57BL/6 retinas. Light flashes reliably triggered depolarizations in OBCs (Fig. 3G red trace) as opposed to the hyperpolarizations observed in *rd1* OBCs (Fig. 3G, black trace). Inversion of the signal is a clear indicator that Mela(CTmGluR6) acts through the mGluR6 signaling cascade. Glutamate is naturally released from the photoreceptors in the dark to activate mGluR6 while Mela(CTmGluR6) is inversely activated by light (Suppl. Fig. 5)[5]. While Mela(CTmGluR6)-driven OBC responses from the whole mount *rd1* retina were overall slower compared to photoreceptor-driven OBC responses recorded from dark-adapted C57BL/6 retinal slices (n=6; wild-type TauON: 111 ± 34.3ms, p=0.0055; wild-type TauOFF: 266.8 ± 167.4ms, p=0.0125; Fig. 3H), there was some overlap, with several Mela(CTmGluR6)-driven responses reaching the speed of wild-type responses. The larger scatter of kinetic values in Mela(CTmGluR6) transduced *rd1* retinas likely reflects the variability in opsin expression within individual OBCs. To investigate how much "drive" Mela(CTmGluR6) can generate in OBCs of the *rd1* retina compared to the natural drive from photoreceptors, we compared the average response amplitudes in both scenarios. Light triggered changes in membrane potential were significantly larger in OBCs of the wild-type retina (9.4 ± 2.8 mV, n= 6) compared to the *rd1* retina (4.7 ± 3 mV, n = 9, p = 0.0087), but responses driven by Mela(CTmGluR6) notably reached about 50% of the wild-type amplitude (Fig. 3I). When considering the many pathological changes in the *rd1* retina, these data were encouraging.

2.4. Detailed functional characterization of optogenetically restored retinal ganglion cell responses

We next characterized the RGC light-responses in the fully degenerated *rd1* retina elicited by Mela(CTmGluR6). We used cell-attached patch-clamp recordings in whole mount retinas in combination with dye-injection to serve subsequent morphological identification of the RGC type and identified all cardinal RGC response types (Fig. 4A): ON-sustained (ON-S), ON-transient (ON-T), OFF-sustained (OFF-S), OFF-transient (OFF-T) and the ON-OFF type. Finding ON-response types whilst eliciting hyperpolarizing responses in OBCs by Mela(CTmGluR6) confirms functional signaling through AII amacrine cells (Suppl. Fig. S5). Segregation of transient and sustained response types further infers a broadly restored inhibitory amacrine cell circuit within the inner retina. Remarkably, the diversity of RGC response types was preserved in retinas from very old *rd1* mice tested, indicative that the optogenetic treatment may stabilize or slow down the degenerative process (Suppl. Fig. S6).

We next compared the response latencies of ON and OFF type RGCs in the wild-type and Mela(CTmGluR6)-treated *rd1* retinas. As for Mela(CTmGluR6)-driven responses in OBCs of the *rd1* retina, latencies were significantly attenuated and showed increased jitter (ON-RGCs: 0.23 ± 0.12 s, n=17; OFF-RGCs: 0.35 ± 0.24 s, n=7) compared to wild-type retinas (ON-RGCs: 0.06 ± 0.02 s, n=8, $p<0.05$; OFF-RGCs 0.05 ± 0.02 s, n=12, $p<0.001$; Fig. 4B). To investigate if response attenuation was due to degeneration-induced changes within the inner retina, such as cell death and rewiring[28], we also treated C57BL/6 mice with Mela(CTmGluR6). To isolate Mela(CTmGluR6)-mediated RGC responses in wild-type retinas, we blocked photoreceptor input pharmacologically with LAP-4 and by high intensity light bleaching[5]. As evident from figure 4B, RGC response latencies of Mela(CTmGluR6)-mediated light responses in wild-type retinas were not significantly different to photoreceptor-mediated responses (ON-RGCs: 0.04 ± 0.01s, n=4; p=0.71). These results infer that progressing retinal degeneration, including potential neuronal rewiring[5,27], affects signal propagation within the inner retina, and that the Mela(CTmGluR6) *per se* restores normal retinal signaling kinetics.

Comparing the overall distribution of RGC response types in treated *rd1* and wild-type retinas it became evident that ON-responses dominate in the treated *rd1* retina (68.7% ON and 25.7% OFF, n=37), whilst ON and OFF responses show a more balanced distribution in the wild-type retina (ON: 44.7%, OFF: 47.4%, n=35, Fig. 4C). Another difference observed in the treated *rd1* retina was a marked increase in transient responses (transient: 48.6%, sustained: 45.7%) compared to the wild-type retina where sustained responses dominated (26.6% transient and 65.8% sustained). We interpret transientness as a consequence of strong activation of the inhibitory amacrine cell circuitry that truncates RGC responses.

Dye injection after recordings allowed subsequent anatomical identification of RGCs according to their arborization patterns in the distal and/or proximal stratum of the inner plexiform layer (Fig. 5). Interestingly, only 37% of the RGCs had an inverse response polarity with respect to their anatomy and these cells were predominantly native OFF-RGCs (see also Supplementary Table S2). These results explain the accumulation of ON responses in the treated *rd1* retina compared to the wild-type retina. Since similar experiments in treated C57BL/6 mice previously showed a more consistent inversion of light response polarity[5], we interpret the partial lack of sign-inversion in the *rd1* retina as pathological changes within the amacrine cell network [32].

The single-cell patch-clamp data was supported by multi-electrode array (MEA) recordings from retinal flat-mounts of treated *rd1* mice. Significantly more RGCs exhibited light responses in Mela(CTmGluR6)-treated *rd1* retinas (50.8 ±1 7.4 %, n= 24; p=0.004) compared to untreated *rd1* controls (28.3 ± 14.6 %, n= 7 retinas; Fig. 6A) and the number of light-responsive cells did not statistically differ from healthy C57BL/6 retinas (68.6 ± 33.4 %, n=6, p=0.077). Unsupervised spectral clustering of the recordings from dark-adapted Mela(CTmGluR6)-treated *rd1* retinas revealed the six distinct RGC types known in wild type C57BL/6 retinas (Fig. 6B), with about 65% of them starting to respond during light stimulation (ON responses) and 35% after light stimulation (OFF responses; Suppl. Fig. S7A). These quantitative results support the more qualitative patch-clamp experiments and confirm the restoration of all cardinal retinal light response types in the optogenetically treated *rd1* retina, OFF and ON responses with different kinetic properties (transient vs. sustained). Kinetically slower ipRGC-like light responses were also found in treated *rd1* retinas (Fig. 6B, Suppl. Fig. S7B; Tau ON= 1.55 ± 0.26 s) and did not significantly differ from ipRGC responses observed in untreated *rd1* controls (1.43 ± 0.42 s; p=0.078). The same unsupervised response clustering was also performed on healthy controls and untreated *rd1* animals and yielded 7 and 2 response clusters, respectively (Suppl. Fig. S7C&D). The peak firing frequencies in Mela(CTmGluR6)-treated *rd1* retinas were also similar to those in healthy C57BL/6 retinas ($5x10^{14}$ photons/cm^2/s; > 58 Hz; p = 0.4058) and significantly higher than those seen in untreated *rd1* controls (p=0.013; Suppl. Fig. S7E). These observations may explain, at least in part, the high contrast sensitivities restored in the OMR recordings. We did not observe significant differences in response distributions between retinas from younger or older treated *rd1* animals (Suppl. Fig. S7F; p=0.703).

Another fundamental property of vision is the ability to adapt retinal responsiveness to the range of ambient light intensities. We wondered whether light adaptation was still present in the optogenetically treated *rd1* retinas. For this,

we generated dark- and light-adapted (15 min white light, 100 μW cm^{-2}) intensity-response curves from RGCs by exposing retinas to a series of brief 470nm light flashes of increasing intensities. The dark-adapted intensity–response curve was in good agreement with previous data from single-cell RGC patch recordings[5] (Fig. 6C). The light-adapted curve showed a shift of more than 1 log unit on the intensity axis, representing the light adaptive capability of the optogenetically restored inner retina. We also observed significantly higher spiking frequencies in the light adapted retina when using light intensities beyond the half-saturation values (Suppl. Fig. S7G). Overall, the Mela(CTmGluR6)-expressing *rd1* retina responds over 6 log units of light intensities (10^{10}-10^{16} photons/cm^2/s), to our knowledge the widest range reported for optogenetic restoration of light sensitivity.

2.5. Behavioral pattern vision and restoration of cortical light responses

The OMR is a reflex elicited by a subset of direction selective ganglion cells (DSGCs) that project to the accessory optic system - and not via the lateral geniculate nucleus (LGN) to the primary visual cortex (V1). We therefore also probed cortical image forming vision behaviorally. We employed a conditioned visual task in which the mouse had to distinguish drifting gratings of the highest acuity achieved in the OMR, 0.35 cyc/deg (100% contrast, rotation speed 12°/s) from equiluminescent gray. The mice were conditioned in a custom-made plexiglass shuttle-box consisting of two identical adjoining compartments connected by a small opening (Fig. 7A). Each compartment was equipped with a computer monitor that displayed either gray with a luminance equivalent to the OMR ($5x10^{13}$ photons/cm^2/s) or an equiluminescent drifting grating (0.35 cyc/deg). On the first day, mice were habituated to the shuttle-box. (Fig. 7A). During a 2-day training period, the screen switched three times every 5 minutes from gray to the equiluminescent pattern stimulus in the compartment where the mouse resided at the time. The stimulus was paired with an aversive foot shock in that same compartment. On day 4 the electric grids were removed and the odor as well as the orientation of the shuttle-box changed to avoid environment-induced conditioned fear behavior. The drifting grating was displayed on the side where the mouse resided after a 5 min habituation period. Aversive behavior during the display of the pattern stimulus was compared to the baseline aversive behavior before stimulus onset to get a measure for the behavioral change as a consequence of pattern recognition. Mela(CTmGluR6)-injected *rd1* mice (n = 9) displayed strong visually-cued aversive behaviors similar to wild-type C57BL/6 mice (n=6, p=0.9935, ANOVA with post-hoc Tukey). Stimulus-triggered changes in adverse behavior was absent in untreated *rd1* littermates (n=5, $p < 0.001$, Fig. 7B). The increase of aversive behavior in response to the visual cue was highly significant in Mela(CTmGluR6)-treated (p=0.0003) and C57BL/6 mice (p=0.0026), but no behavioral change in response to the drifting stimulus was seen in untreated *rd1* littermates (p=0.9999, Fig. 7C).

From the same mice we subsequently recorded visually evoked field potentials (VEPs) from layer 4 of V1. A 500 ms blue light stimulus of similar light intensity employed in the OMR and open field box paradigm (5×10^{13} photons/cm^2/s) was supplied to the contralateral eye. We compared responses from Mela(CTmGluR6)-treated and non-treated *rd1* mice older than 280 days of age when V1 was shown to no longer respond to visual stimuli in *rd1* mice[1]. In addition, we recorded VEPs from C57BL/6 dark- and light-adapted mice. VEPs were reliably evoked in C57BL/6 (both dark- and light-adapted) and Mela(CTmGluR6)-treated *rd1* mice, but not in non-treated *rd1* littermates (Fig. 7D). VEPs from Mela(CTmGluR6)-treated *rd1* mice were similar in amplitude (611.8 ± 376.1μV) to the VEPs of light-adapted C57BL/6 retinas (366.9 ± 89.8μV; p=0.043; Fig. 7E). This aligns with previous studies showing that light-adapted VEPs in the mouse have a smaller amplitude compared to dark-adapted VEPs[34]. The response latencies of Mela(CTmGluR6)-treated *rd1* mice (555.6 ± 26.6 ms), however, were significantly increased compared to the response latencies of both, dark-adapted (132.4 ± 17.7 ms, $p < 0.0001$) and light-adapted C57BL/6 mice (107.8 ± 28.8ms, $p < 0.0001$; Fig. 7F). To investigate if this delay was due to retino-cortical signal processing or originated in the degenerating retina, we performed MEA recordings on Mela(CTmGluR6)-treated *rd1* retinas with matched light intensities ($5x10^{13}$ photons/cm^2/s, see Fig. 6C & Suppl. Fig. S7G). Under these conditions we elicited robust, but delayed RGC light responses with latencies similar to the VEPs measured under the same conditions (481 ± 254 ms; n=41, p = 0.173; Fig. 7F). This provides evidence that the delay of VEPs in V1 of treated *rd1* mice is an effect of retinal degeneration and not due to altered retino-cortical signaling in the *rd1* mouse.

3. Discussion

Optogenetic gene therapies are in clinical trials to restore vision in blind patients (ClinicalTrials.gov Identifier: NCT03326336, NCT02556736, NCT04278131). Recently, a milestone was reached when one patient with advanced retinitis pigmentosa that was treated with a therapy introducing the microbial channelrhodopsin, ChrimsonR, into the RGCs has regained the ability to locate and count objects[35]. Due to the very high light intensities required for ChrimsonR

activation, the patient was additionally equipped with biomimetic goggles amplifying and spectrally-adapting the ambient light. Multiple approaches are currently under development with the goal to further improve the quality of optogenetically restored vision. Since neural processing within the retina extracts approximately 30 parallel information channels from the visual scene[6], endeavors are made to restore inner retinal processing by direct optogenetic targeting of inner retinal cells. Retinal processing is mostly lost when turning RGCs into "replacement photoreceptors" using an optogenetic actuator. Therefore, OBCs, the first order retinal interneurons, are undoubtedly attractive targets for optogenetic vision restoration, since they feed the light signal into the inner retinal circuitry and thereby maximize the receptive-field diversity within the RGC population. OBC-targeted optogenetics was recently made possible by molecular advances that allow efficient and selective OBC targeting[7], despite OBCs being rather non-permissive to AAV transduction[36].

In this study we investigated the potential of OBC-targeted optogenetic vision restoration in detail. We confirm that activation of OBCs restores inner retinal signaling and with that, RGC receptive-field diversity, an important building block for high quality vision. We focused on chimeric Opto-GPCRs that efficiently activate the native mGluR6 signaling cascade[5,37] , making them 3-4 log units more light sensitive compared to their microbial counterparts (i.e. ChRs). We compared four Opto-GPCRs: Opto-mGluR6[5], OPN1MW-mGluR6[4,7] and two new melanopsin/mGluR6 chimera variants with only the C-terminus (Mela(CTmGluR6)), or the C-terminus and IL3 (Mela(CT+IL3mGluR6)) replaced by that of mGluR6. Whilst C-terminal replacement facilitated subcellular trafficking and efficient expression, exchanging the IL3 domain appeared to compromise opsin function and/or expression. Although additional replacement of IL2 in melanopsin, as in Opto-mGluR6, further reduced the currents elicited in HEK293 cells (see Figs. 1B,C), this almost complete chimera design appeared to optimize coupling to Gαo, as evident from the well restored OMR (see Figs. 1H,I). As shown previously, additional replacement of IL1 did not improve function or Gαo coupling in Opto-mGluR6[5]. Opto-mGluR6 and Mela(CTmGluR6) both restored high contrast and spatial vision in treated *rd1* mice, with Mela(CTmGluR6) outperforming Opto-mGluR6 in the restoration of visual acuity, with some mice reaching performances of C57BL/6 mice. One possible explanation for the diverging results for Opto-mGluR6 in the HEK293-GIRK patch-clamp experiments and the *in vivo* OMR experiments is that HEK293-GIRK cells do not express the Gαo type G-protein and may therefore not accurately predict coupling to the mGluR6 pathway targeted in OBCs *in vivo*[38,39]. Opto-mGluR6 with the most complete mGluR6 intracellular domain exchange may couple very well into the Gαo pathway of OBCs, but less successfully into the Gαi pathway present in HEK293 cells. In this respect, the high complexity of GPCR signaling and regulation, which depends on the intracellular complement of cell-specific binding partners, may advocate the use of chimeric Opto-GPCRs over non-engineered opsins[11]. On the other hand, extensive chimera design may compromise opsin function. Our data show that the minimally chimeric Mela(CTmGluR6) has good Gαo coupling, expression and function. It is evident that Mela(CTmGluR6) efficiently activates the Gαo pathway within retinal OBCs, since: (1) The polarity of the Mela(CTmGluR6) signal in OBCs is inverted (hyperpolarizing) compared to the photoreceptor-driven light signal in the C57BL/6 retina (depolarizing), a consequence of direct Gαo light activation [40,41] (see Fig. 3G), (2) the restored light-responses are kinetically similar to those recorded in healthy C57BL/6 retinas (see Fig. 3H), (3) Mela(CTmGluR6) elicited cell-subtype specific light-responses in isolated rod and cone OBCs, i.e. sustained vs. transient responses, indicative of activation of different endogenous signaling pathways as a result of differences in the molecular mGluR6 cascade elements in different OBC types (see Fig. 3C,D). Although temporal filtering continues in the inner retina, this early segregation of information into separate temporal channels supports the diversity of RGC output and is lost when expressing microbial opsins (e.g. ChR2) in the OBCs. At the RGC level, Mela(CTmGluR6) restored all cardinal RGC response types (ON-S, ON-T, OFF-S, OFF-T, ON-OFF) in response to a full-field light stimulus, indicative of sufficient optogenetic drive at the OBC level to efficiently activate the inner retinal circuitry.

We confirmed that Mela(CTmGluR6) trafficked to the macromolecular mGluR6 cascade complex in the OBC dendrites and co-localizes with Gαo and the effector channel TRPM1, fundamental for successful restoration of Gαo signaling in OBCs. The kinetics of optogenetically-elicited light-responses in OBCs were near to that of endogenous mGluR6. We speculate that this was achieved through Mela(CTmGluR6)'s ability to drive specific mGluR6 activity regulators, such as RGS proteins, Ca^{2+} binding proteins, GRKs and arrestins resident within OBCs.

The native light intensity integrator and circadian master clock entraining function of melanopsin is relatively slow, which so far reduced melanopsin's attractiveness for optogenetic control of precise neuronal activity[42]. However, we here show that truncated and C-terminally adapted melanopsin is an excellent and fast optogenetic tool as evident from the fact that Mela(CTmGluR6) supported vision at high spatial acuity in the OMR and open field box.

We based chimeras on melanopsin because cone opsin bleaches and depends on the visual cycle within the retinal pigment epithelium, which is often compromised in retinal degeneration. Melanopsin, similar to microbial opsins and some non-ciliary G-protein coupled opsins is bleach resistant, with a closed-loop photocycle that re-isomerizes the dark-

state chromophore[43,44]. Consequently, and as shown, the activity of melanopsin does not decrease upon repeated stimulation in the presence of long-wavelength light (595nm). Temporally controllable light-modulation of the ON and OFF states makes melanopsin - and non-bleachable opsins in general - particularly attractive tools for optogenetic applications.

While the spike latencies and spike firing rates in RGCs produced by Mela(CTmGluR6)-input to OBCs of non-degenerated mice were similar to those elicited by photoreceptor input, latencies of light responses were significantly attenuated in the degenerated *rd1* retina, not only in the RGCs but also in V1. Our results point towards functional adaptations within the inner retina during the degenerative process. Indeed, previous anatomical studies showed that bipolar cells undergo remodeling in later stages of degeneration, including changes in morphology, synaptic connectivity and receptor expression[28,45-47]. However and notably, our data hints towards a potential stabilization of the degenerative process in the *rd1* retina upon optogenetic treatment, since the restorative outcome did not deteriorate with time after treatment (see Suppl. Figs. S6, S7F). This may indicate a protective effect of optogenetic activation; however, proving this would require further experiments.

We observed an accumulation of ON-type and transient RGC responses in the treated *rd1* retina. This was surprising since optogenetic activation of OBCs with Mela(CTmGluR6) leads to a hyperpolarization of OBCs corresponding to OFF responses in native ON-cells. The shift to more ON-type responses reflects our finding that OFF-RGCs mostly undergo sign-inversion, as demonstrated by the dendritic stratification patterns of recorded cells. Since ON-RGC responses are indirectly generated via AII amacrine cells (Suppl. Fig. S5), our findings confirm successful recruitment of the AII circuit. We interpret transientness to be a consequence of strong activation of the inhibitory amacrine cell circuitry within the inner retina that acts to truncate the RGC response[48]. Interestingly, an increase in transientness of RGC output was previously reported in a study where ChR2 was expressed in OBCs[3]. This suggests that strong inhibitory feedback may be a feature of the degenerated retina. The Mela(CTmGluR6) treated *rd1* retina also regained some ability to adapt to ambient light levels, which we also attribute to inner retinal circuits (Fig. 6C). Adding to these findings, the restoration of the OMR in treated *rd1* mice may infer more complex direction-selective circuits, although not proven here.

In summary, we find the restorative outcomes achieved by OBC-targeted optogenetic gene therapy encouraging, particularly since the encoding capacity of the inner retina appears to be largely preserved after optogenetic treatment, albeit with small variations. Our findings are particularly interesting from a translational point of view, since they allude to improved strategies for optogenetic intervention. Nevertheless, extrapolation of results from mice to human patients should be done with caution.

4. Materials and Methods

4.1. Plasmid generation and HEK293-GIRK whole-cell patch-clamp experiments

The Kir2.1 membrane trafficking signal (TS) as well as the rhodopsin trafficking sequence (1D4 epitope) were added to all parent opsins and opsin-mGluR6 chimeras. All opsins were cloned into a pIRES2_melanopsin-mGluR6_TurboFP635 plasmid[5] that was modified to contain the fluorescent protein mKate2 in place of the IRES-TurboFP635 sequence. A stable HEK293-GIRK1/2 cell line (kind gift from Olivia Masseck) was transiently transfected with the opsin constructs to identify current responses by whole-cell patch-clamp in a high potassium extracellular solution triggered by a light stimulus generated by a pE-4000 system (CoolLED, Andover, United Kingdom). Traces were analyzed offline using Igor Pro software (Wave Metrics).

4.2. Animals and AAV transduction

The opsin-mGluR6-TS-1D4 variants were recloned into the pAAV-770En_454P(h*GRM6*)-*Opn1mw*-CTmGluR6-TS-1D4-IRES2-TurboFP635-WPRE-BGHpA plasmid[7] and packaged into an AAV2(7m8) vector[24]. C3H/HeOuJ (rd1) and C57BL/6J mice were bilaterally and intravitreally injected (2.5µl, $1x10^{12}$ - $5x10^{13}$ vg/ml) using a 33G blunt needle. Animal experiments and procedures were in accordance with the Swiss Federal Animal Protection Act and approved by the animal research committee of Bern (approval number BE99/19).

4.3. Retinal patch-clamp recordings

Bipolar cells were patch-clamped with electrodes of 8–10MΩ using the perforated, cell-attached method either in whole mount retinas (rd1), in slices, or after acute dissociation. The methods for recoding cell-attached light responses from RGCs have been described in detail previously[5]. All recordings were made using a HEKA EPC10 amplifier with

PatchMaster software and performed at 34–36°C. RGCs were labelled by addition of 0.2% biocytin (Sigma) to the intracellular solution.

4.4. Immunohistochemistry

In brief, retinas were fixed in 4% paraformaldehyde in 0.1M phosphate buffer (pH 7.4) for 30 min. Sections were incubated overnight at 4°C in primary antibody and 2h in secondary antibody at room temperature. The following primary antibodies were used: rabbit anti-tRFP (1:1000; Evrogen; AB234), goat anti-melanopsin (1:1000; Advanced Targeting Systems; AB-N39), goat anti-ChAT (1:100; Millipore; AB144P) and mouse anti-Goα (1:1000; Millipore; mab3073). Alexa 488 conjugated to streptavidin was used to visualize cells injected with biocytin (1:400; Invitrogen; S-11223). Nuclei were stained with 10µg/ml DAPI (Roche). Micrographs were taken on a Zeiss LSM 880. Processing of image stacks was done using ImageJ (Rasband WS, United States National Institutes of Health, Bethesda, Maryland, US).

4.5. Multi-electrode Array recordings

Retinas were placed with the RGC side on multi-electrode arrays (60MEA200/30iR-Ti; Multi Channel Systems MCS GmbH) and placed into the MEA recording device (MEA2100-System; Multi Channel Systems MCS GmbH). Light stimulation was performed with a pE2 light stimulator (precisExcite, CoolLED, Andover, United Kingdom, 465 nm, 5 x 10^{14} photons/cm^2/s unless stated otherwise). Recordings were performed at 34°C and collected, amplified, and digitized at 25 kHz using MCRack software (Multi Channel Systems MCS GmbH). Single cell spike occurrences were extracted offline using Matlab (MathWorks). For dose-response curves, isolated retinas were dark-adapted for 20 min and subsequently tested in a series of brief (500 ms) blue light flashes (470nm) at 120-s intervals over a range of intensities. Retinas were then adapted for 15 min to a moderate indoor light levels (white light, 100 µW cm^{-2}) and retested as described above.

4.6. In vivo electrophysiological recordings from the visual cortex V1

Mice were anesthetized by an intraperitoneal (IP) injection of ketamine and xylazine and subsequently mounted in a stereotaxic device (David Kopf, USA). The pupil of the stimulated eye was dilated with a drop of 10 mg/ml atropine sulphate (Théa Pharma) and a craniotomy ~ 1 mm in diameter was made over the left occipital cortex. The electrode was inserted 1.5-2.5 mm lateral and 0.1-0.5 mm rostral to lambda into V1. The tungsten microelectrodes (WE3PT30.01A5, Microprobes) had an impedance of 9-15 kΩ and were guided diagonally through the V1 to reach layer 4 using a micromanipulator and stereomicroscope (Amscope). After insertion of the electrode, mice were dark adapted for 30 minutes. For the light stimulation paradigms we used Samsung Sync master 940b LCD display (60 Hz refresh rate, luminance 5 x 10^{13} photons/cm^2/s) located 20 cm away from the eye. Signals were acquired, amplified and digitized at 20 kHz with the RHD 2000 system from Intan Technologies. Recordings were analyzed offline using Matlab. Bar plots are shown as means ± SD, exemplar traces as means ± s.e.m.

4.7. Optomotor Reflex Measurement

We employed Striatech's virtual optomotor system to assess the spatial frequency and contrast thresholds of rd1 mice >p168 of age, when no OMR responses remain in untreated animals[5,25]. Tracking head movements were bilaterally recorded by an infrared-sensitive digital camera and analyzed using the OptoDrum software (Striatech, v.1.2.8). The rotation speed was kept constant at 12°/s, which was shown to elicit an optimum response under photopic conditions[49]. Visual acuity was examined with a stair-step protocol of increasing spatial frequencies (100% contrast) and threshold defined as the highest grating frequency that can evoke animal head tracking[26,50]. Contrast sensitivity, the inverse of the Michelson contrast [C = (I max − I min)/(I max + I min)] was determined analogously at 0.125 cyc/deg spatial frequency, where injected rd1 mice performed best (Suppl. Fig. 2). Data was obtained by three independent experimenters on 3-5 separate measurement days.

4.8. Open-field box experiments

Experiments were performed in a two-compartment shuttle-box (27.5 x 30.5 x 35 cm) connected by a 6 x 5.5 cm gate (Fig. 7A) with rd1 mice >p280 of age, when no cortical responses to pattern stimuli can be observed[5]. The floors were equipped with removable shock grids (Med Associates Inc, Model VFC-005A) to administer electric foot shocks during cued fear conditioning on days 2-4 (Fig. 7A). At the two opposite short walls of the setup, computer screens (SAMSUNG

SyncMaster 940B, Type: GH19PS, width: 38 cm, height: 30.5 cm) were mounted run by a script on Noldus software (EthoVision XT, Version 11), providing equiluminescent gray or moving gratings of 0.35 cyc/deg spatial frequency (100% contrast, speed 12 deg/s). Behavior was video recorded with an IR-sensitive BASLER camera (Model acA1300-80GMnir). The experiment consisted of four sessions on four consecutive days (8:00-12:00 am) as described in Fig. 7A. Aversive behavior (freezing, residing in the opposite compartment, jumping or tail rattling) was manually scored as cumulative time in for 1 minute before the onset of the pattern stimulus (baseline) and 1 minute during stimulus presentation.

4.9. Statistics

For patch-clamp recordings Student`s t-tests was used. For MEA and cortical responses, either unpaired 2-tailed Student's t-test or 2-tailed Kolmogorov-Smirnov test with Bonferroni correction was used. If not stated otherwise, mean ± SD are given.

Behavioral data was analyzed with a one-way ANOVA for multiple comparisons with post hoc analysis with Tukey's honestly significant difference (HSD) of means in R v.3.6.0. Assumptions of normality were not rejected by the Shapiro-Wilk normality test and homogeneity of variance was tested with the Levene's or the Bartlett test. Data is depicted as boxplots indicating the median ± standard deviation.

In graphs, the significance levels are indicated as $p \leq 0.05$, $p \leq 0.01$, and $p \leq 0.001$.

A detailed Materials and Methods section is given in the Supplementary Material.

Author Contributions: Conceptualization, SK; methodology, SK, MvW and JK; software, JK; formal analysis, SK, MvW and JK; investigation, MvW, JK and NS; resources, SK; writing original draft preparation, SK; writing—review and editing, SK, MvW and JK; supervision, SK; project administration, SK; funding acquisition, SK.

Funding: This research was funded by the Swiss National Science Foundation (31003A_152807 and 31003A_176065), the Bertarelli Foundation (Catalyst fund, project BCL7O2), the Haag-Streit Holding AG and Arctos Medical AG.

Institutional Review Board Statement: Animal experiments and procedures were in accordance with the Swiss Federal Animal Protection Act and approved by the animal research committee of Bern (approval number BE99/19).

Data Availability Statement: The datasets used and/or analyzed during the current study are available from the corresponding author upon reasonable request.

Acknowledgments: We would like to thank Matti Zbinden and Simon Hostettler to help perform behavioral experiments, Günther Zeck and Ludovic Mure for fruitful advice and discussions on retinal multi-electrode array recordings, Anwesha Bhattacharyya for advice on cortical recordings, Giulia Schilardi for support in the immunohistochemistry and Christian Dellenbach and Hans Ruchti for electronic support. We also thank Sabine Schneider for her excellent support in cloning, viral packaging and histology and Michael Känzig for taking care of the animals.

Conflicts of Interest: SK and MvW are inventors on the patent application P180999CH00 that discloses the chimeric proteins Mela(CTmGluR6) and Mela(CT+IL3mGluR6).

Figure legends

Figure 1. *In vitro* and *in vivo* screening of opsin constructs. (A) HEK293-GIRK cells transiently transfected with different Opsin-mKate fusion proteins show robust membrane expression (exemplified for OPN1MW(CT mGluR6)-mKate and Mela(CTmGluR6)-mKate). (B-H) To assess the relative efficacies at which opsin constructs activate G-proteins in the Gαi/o class, we screened all opsin constructs in HEK293-GIRK cells. (B) Example light responses recorded in HEK293-GIRK cells (stimulus presented by blue bar; 470nm; 10^{14} photons/cm^2/s). (C) Average normalized GIRK response amplitudes recorded under the same conditions as in B. Substituting the C-terminus with that of mGluR6 resulted in significantly larger GIRK responses to light in melanopsin (p=0.0008) and OPN1MW (p=0.0159). (D&E) The relative Tau ON (D) and Tau OFF (E) values of the different opsins in HEK293-GIRK cells using similar data to that presented in B. Although not significant, we observed a slight tendency towards shorter Tau ON values in constructs that generated larger response amplitudes (D). Tau OFF values did not differ significantly, with the exception of

melanopsin chimeras recorded with an orange backlight (E; 595nm at 5 x 10^{15} photons/cm^2/s; p = 0.0008). (F&G) Repetitive light stimuli (5 sec duration at 1min intervals; 470nm; 5 x 10^{13} photons/cm^2/s) in GIRK cells transfected with OPN1MW(CTmGluR6) (F; green) and Mela(CTmGluR6) (F&G; black). Since melanopsin is tri-stable, we observed no bleach run-down when using an orange backlight (G; 595nm at 5 x 10^{15} photons/cm^2/s). This response showed little attenuation, even at 0.2 Hz stimulation (blue arrow; insert). (H & I) *In vivo* screening of treated blind (>24 weeks) *rd1* mice in a naïve optomoter reflex task. (H) Visual acuity thresholds: all opsins restore visual acuity significantly in blind *rd1* mice, with Mela(CTmGluR6) significantly outperforming the other constructs [n(rd1) = 15 (negative blind control), n(rd1_Opto-mGluR6) = 12, n(rd1_Mela-mGluR6(CT) = 16, n(Mela-mGluR6(CT+IL3) = 5, n(OPN1MWW-mGluR6(CT) = 5, n(C57BL/6) = 10 (positive seeing control)]. (I) Contrast Sensitivity thresholds: Mela(CTmGluR6) and Opto-mGluR6 significantly outperform the other constructs, with average contrast sensitivity values for Mela(CTmGluR6) treated mice not being significantly different to those determined in C57BL/6 mice. Since *rd1* mice were unable to track at 100% contrast, they are not shown in this graph.

Figure 2. Targeted expression in OBCs after intravitreal injection. (A) A representative *rd1* retina four weeks after intravitreal injection of Mela(CTmGluR6)-IRES-TurboFP635. Inserts show higher magnification scanning micrographs taken from the bipolar cell layer at specified regions, with relatively high (1) or low (2) transduction. Despite the highlighted heterogeneity, OBCs were transduced across the retina. (B) Expression was specific for OBCs in the *rd1* retina (TurboFP635 in green; Gαo in red; DAPI in blue). (C) A Mela(CTmGluR6)-mKate fusion protein demonstrates robust targeted expression to the OBC dendrites (mKate in green; Gαo in red; DAPI in blue). Scale bars 500μm in A and 50μm in other panels.

Figure 3. Mela(CTmGluR6) driven light responses in OBCs. (A) We targeted isolated OBCs for electrophysiological recordings by their characteristic morphology under IR-DIC optics and reporter gene expression. (B) Isolated rod bipolar cells responded with a small but consistent hyperpolarization to light (470nm; 10^{14} photons/cm^2/s; trace shows average response of 6 cells with shaded area indicating 1 SD). (C) An isolated cone OBC with a fast, biphasic response to the same light stimulus presented in B demonstrates diverse intrinsic processing within different OBC types. (D) In whole mount *rd1* retinas, OBCs were targeted for recording by reporter gene expression and by the characteristic size and location of their cell bodies. (E&F) Recordings from transfected rod bipolar cells in the whole mount *rd1* retina had robust light responses with a faster recovery time compared to isolated cells (E; 470nm; 10^{13} photons/cm^2/s) and could be repeatedly triggered at 0.4 Hz (F). (G) Light responses from a transduced rod bipolar cell in a *rd1* whole mount retina (black) compared to a light response form a rod bipolar cells in a wild type C57BL/6 slice preparation of the retina (red; 470nm; 1 x 10^{13} and 1 x 10^{11} photons/cm^2/s, respectively). (H) Tau ON and Tau OFF values of wild type OBCs (n=6) and Mela(CTmGluR6)-transduced *rd1* OBCs (n=9). Although time constants recorded from wildtype cells were on average faster, both, the ON and OFF time constants of some treated cells overlapped with those recorded from wildtype cells (p = 0.0055 and 0.0125, respectively). (I) Average response amplitudes of the same responses presented in G. Scale bars in A and D 50 μm.

Figure 4. Mela(CTmGluR6) restores diverse receptive-field types in the RGC population of the degenerated *rd1* retina. (A) Extracellular recordings from RGCs in the Mela(CTmGluR6)-treated *rd1* retina during light stimulation reveal all canonical receptive-field types: transient ON (ON-T), transient OFF (OFF-T), sustained ON (ON-S), sustained OFF (OFF-S), ON-OFF as well as melanopsin responses from ipRGCs. (B) The response onset of ON and OFF RGCs in treated *rd1* retinas had a relatively wide scatter compared to the WT retina. (C) Pie-charts showing the relative fraction of receptive-field types (excluding melanopsin) recorded in the WT and the Mela(CTmGluR6)-treated *rd1* retina. Compared to the WT retina, we observed a relative shift from OFF to ON response types and from sustained to transient responses in the treated *rd1* retina.

Figure 5. Anatomy-function correlation of Mela(CTmGluR6)-triggered RGC responses in the treated *rd1* retina determined by patch-clamp. Anatomy and corresponding light responses of 4 example RGCs from Mela(CTmGluR6)-treated *rd1* retinas show that some native OFF RGCs (A&B) have inverted light responses (i.e. dendrites that stratify in the OFF sublamina of the inner plexiform layer (IPL) with a light response at the onset of light), while the light responses of other cells (C&D) are not inverted (i.e. cells that stratify in the OFF sublamina of the IPL respond at the end of the light stimulus). Also see Supplementary Table S2. Light stimulus indicated as blue bar above spike trains (470nm; 10^{14} photons/cm^2/s). Scale bars = 100µm.

Figure 6. Compound RGC responses in retinas from Mela(CTmGluR6)-treated *rd1* mice determined on multi-electrode arrays. (A) We observed a significantly higher percentage of responsive cells in treated *rd1* retinas (n=24) compared to untreated *rd1* retinas (n=7, p=0.0044). There was no significant difference in percentage of responsive cells between C57BL/6 retinas (n=6) and Mela(CTmGluR6)-treated *rd1* retinas (p=0.077). (B) Example average traces of different functional RGC categories. Light stimulation (470nm, $5x10^{14}$ photons/cm^2/s, 1s) indicated as blue bars. Below each representative average trace (mean ± s.e.m.) is a heat map of representative individual cells. (C) Dark-adapted (black trace) and light-adapted (dark yellow trace) intensity response curves from RGCs of Mela(CTmGluR6)-treated *rd1* retinas (n=69 cells). Cells were stimulated every 120s with a blue light flash (470nm, $1.12x10^{10}$ – $2.5x10^{16}$ photons/cm^2/s), light adaptation for 15 minutes (white light at 100 µW cm^{-2}) and then the stimulation protocol was repeated. I_{50}(dark-adapted) = 3.65 x 10^{14} photons/cm^2/s, I_{50}(light-adapted) = 5.18 x 10^{15} photons/cm^2/s.

Figure 7. Restoration of conditioned visually guided behavior. (A) Graphical depiction of the two-compartment visual conditioning paradigm to a moving grating (0.35 cyc/deg spatial frequency). (B) Comparison of aversive behaviors on day 4 before and during the pattern display increased significantly in C57BL/6 controls (p=0.00263) and Mela(CTmGluR6)-treated *rd1* mice (p=0.00026), while non-treated *rd1* mice did not show a behavioral response to the pattern stimulus. Shown are medians ± SD, red vertical lines denote the means. See movie M1 in the supplementary information for a typical behavior of a treated *rd1* mouse in response to the drifting gratings. Comparsion of 60 seconds pre-stimulus vs. 60 seconds during stimulus. (C) Stimulus-triggered aversive behavior was equally observed in Mela(CTmGluR6) injected *rd1* mice (n=9) and healthy C57BL/6 mice (positive control, n=6; p=0.9935), but not in untreated *rd1* littermates (negative control, n=5; p = 0.00005). (D) Average VEP responses to a full-field light stimulus

(470nm, 5 x 10^{13} photons/cm^2/s, 500 ms) in dark-adapted C57BL/6 animals (n=9 traces), light-adapted C57BL/6 animals (n=6 traces), Mela(CTmGluR6)-treated *rd1* animals (n=22 traces) and untreated *rd1* controls (n=9 traces). (E) Comparison of P1-N1 amplitudes in light adapted C57BL/6 animals (367 ± 90 μV; n=6 traces) and Mela(CTmGluR6)-treated *rd1* animals (612 ± 377 μV; n=22 traces). No significant differences were observed between experimental groups (p=0.043). (F) Comparison of response latencies. The latency was significantly increased in Mela(CTmGluR6) treated *rd1* animals (556 ± 27 ms, n=22 traces) in comparison to dark-adapted C57BL/6 mice (132 ± 18 ms, n=9 traces, p<0.000001) and light-adapted C57BL/6 mice (108 ± 29 ms, n=6 traces, p=<0.000001). No significant difference was observed between dark- and light-adapted C57BL/6 animals (p=0.0596). Latencies of light-intensity matched MEA recordings from RGCs of Mela(CTmGluR6) treated *rd1* mice (481 ± 254 ms; n=41 cells; 500ms; 470nm; 5x10^{13} photons/cm^2/s) did not differ significantly from the V1 latencies in Mela(CtmGluR6) treated mice (p= 0.173). Dots in MEA recordings represent values of individual cells.

References

1 Santos, A. *et al.* Preservation of the inner retina in retinitis pigmentosa. A morphometric analysis. *Arch Ophthalmol* **115**, 511-515 (1997).

2 Cehajic-Kapetanovic, J. *et al.* Restoration of Vision with Ectopic Expression of Human Rod Opsin. *Curr Biol* **25**, 2111-2122 (2015).

3 Lagali, P. *et al.* Light-activated channels targeted to ON bipolar cells restore visual function in retinal degeneration *Nat Neurosci* **11**, 667-675 (2008).

4 Berry, M. H. *et al.* Restoration of high-sensitivity and adapting vision with a cone opsin. *Nature Communications* **10**, 1221, doi:10.1038/s41467-019-09124-x (2019).

5 van Wyk, M., Pielecka-Fortuna, J., Löwel, S. & Kleinlogel, S. Restoring the ON-switch in blind retinas: Opto-mGluR6, a next-generation, cell-tailored optogenetic tool. *PLoS Biol* **13**, e1002143 (2015).

6 Baden, T. *et al.* The functional diversity of retinal ganglion cells in the mouse. *Nature* **529**, 345-350 (2016).

7 Hulliger, E., Hostettler, S. & S, K. Empowering retinal gene therapy with a specific promoter for human rod and cone ON-bipolar cells. *Mol Ther – Methods & Clinic Develop* **17**, 505-519 (2020).

8 Restoring Vision to the Blind: The Lasker/IRRF Initiative for Innovation in Vision Science. *Transl Vis Sci Technol* **3**, 1 (2014).

9 Vardi, N., Duvoisin, R., Wu, G. & Sterling, P. Localization of mGluR6 to dendrites of ON bipolar cells in primate retina. *J Comp Neurol* **423**, 402-412 (2000).

10 Nawy, S. The Metabotropic Receptor mGluR6 May Signal Through Go, But Not Phosphodiesterase, in Retinal Bipolar Cells. *J Neurosci* **19**, 2938-2944 (1999).

11 Koike, C. *et al.* TRPM1 is a component of the retinal ON bipolar cell transduction channel in the mGluR6 cascade. *Proc Natl Acad Sci U S A* **107**, 332-337 (2010).

12 Xu, Y. *et al.* mGluR6 deletion renders the TRPM1 channel in retina inactive. *J Neurophysiol* **107**, 948-957 (2012).

13 Sahel, J.-A. *et al.* Partial recovery of visual function in a blind patient after optogenetic therapy. *Nature Medicine* **27**, 1223-1229 (2021).

14 Rodgers, J. *et al.* Using a bistable animal opsin for switchable and scalable optogenetic inhibition of neurons. *EMBO reports* **22**, e51866 (2021).

15 Emanuel, A. & Do, M. Melanopsin tristability for sustained and broadband phototransduction. *Neruon* **85**, 1043-1055 (2015).

16 Nakajima, Y. *et al.* Molecular characterization of a novel retinal metabotropic glutamate receptor mGluR6 with a high agonist selectivity for L-2-amino-4-phosphonobutyrate. *Journal of Biological Chemistry* **268**, 11868-11873 (1993).

17 Mure, L. *et al.* Melanopsin-Encoded Response Properties of Intrinsically Photosensitive Retinal Ganglion Cells. *Neuron* **90**, 1016-1027 (2016).

18 Tsukamoto, H. *et al.* Retinal Attachment Instability Is Diversified among Mammalian Melanopsins. *J Biol Chem* **290**, 27176-27187 (2015).

19 Kleinlogel, S. Optogenetic user's guide to Opto-GPCRs. *Front Biosci (Landmark Ed)* **21**, 794-805 (2016).

20 Shen, Y., Rampino, M. A., Carroll, R. C. & Nawy, S. G-protein-mediated inhibition of the Trp channel TRPM1 requires the Gbetagamma dimer. *Proc Natl Acad Sci U S A* **109**, 8752-8757 (2012).

21 Law, S., Yasuda, K., Bell, G. & Reisine, T. Gi alpha 3 and G(o) alpha selectively associate with the cloned somatostatin receptor subtype SSTR2. *J Biol Chem* **268**, 10721-10727 (1993).

22 Sun, L. *et al.* Functional assembly of accessory optic system circuitry critical for compensatory eye movements. . *Neuron* **86**, 971-984 (2015).

23 van Wyk, M., Hulliger, E. C., Girod, L., Ebneter, A. & Kleinlogel, S. Present Molecular Limitations of ON-Bipolar Cell Targeted Gene Therapy. *Front Neurosci* **11**, 161 (2017).

24 Dalkara, D. *et al.* In vivo-directed evolution of a new adeno-associated virus for therapeutic outer retinal gene delivery from the vitreous. *Sci Transl Med* **5**, 189ra176 (2013).

25 van Wyk, M., Schneider, S. & Kleinlogel, S. Variable phenotypic expressivity in inbred retinal degeneration mouse lines: A comparative study of C3H/HeOu and FVB/N rd1 mice. *Mol Vis* **21**, 811-827 (2015).

26 Prusky, G., Alam, N., Beekman, S. & Douglas, R. Rapid quantification of adult and developing mouse spatial vision using a virtual optomotor system. *Invest Opthalmol Vis Sci* **45**, 4611-4616 (2004).

27 Jones, B. & Marc, R. Retinal remodeling during retinal degeneration. *Exp Eye Res* **81**, 123-137 (2005).

28 Jones, B. W. *et al.* Retinal remodeling triggered by photoreceptor degenerations. *J Comp Neurol* **464**, 1-16 (2003).

29 Vardi, N., Duvoisin, R., Wu, G. & Sterling, P. Localization of mGluR6 to dendrites of ON bipolar cells in primate retina. *J Comp Neurol* **423**, 402-412 (2000).

30 Xu, Y. *et al.* The TRPM1 channel in ON-bipolar cells is gated by both the α and the $\beta\gamma$ subunits of the G-protein Go. *Sci Rep* **6**, 20940 (2016).

31 Strettoi, E. & Pignatelli, V. Modifications of retinal neurons in a mouse model of retinitis pigmentosa. *Proc Natl Acad Sci U S A* **97**, 11020-11025 (2000).

32 Borowska, J., Trenholm, S. & Awatramani, G. An Intrinsic Neural Oscillator in the Degenerating Mouse Retina. *J Neurosci* **31**, 5000-5012 (2011).

33 Eleftheriou, C. G. *et al.* Melanopsin Driven Light Responses Across a Large Fraction of Retinal Ganglion Cells in a Dystrophic Retina. *Front Neurosci* **14**, 320 (2020).

34 Ridder, W. & Nusinowitz, S. The visual evoked potential in the mouse—Origins and response characteristics. *Vision Research* **46**, 902-913.

35 Sahel, J.-A. *et al.* Partial recovery of visual function in a blind patient after optogenetic therapy. *Nature Medicine* (2021).

36 van Wyk, M., Hulliger, E., Girod, A., Ebneter, A. & Kleinlogel, S. Present molecular limitations of ON-bipolar cell targeted gene therapy. *Front Neurosci* **11**, 161 (2017).

37 Kleinlogel, S., Vogl, C., Jeschke, M., Neef, J. & Moser, T. Emerging approaches for restoration of hearing and vision. *Physiol Rev* **100**, 467-1525 (2020).

38 Dhingra, A. *et al.* Light response of retinal ON bipolar cells requires a specific splice variant of Galpha(o). *J Neurosci.* **22**, 4878-4884 (2002).

39 Law, S., Yasuda, K., Bell, G. & Reisine, T. Gi alpha 3 and G(o) alpha selectively associate with the cloned somatostatin receptor subtype SSTR2. *J Biol Chem* **268**, 10721-10727 (1993).

40 Shen, Y., Rampino, M. A., Carroll, R. C. & Nawy, S. G-protein-mediated inhibition of the Trp channel TRPM1 requires the Gβγ dimer. *Proc Natl Acad Sci U S A* **109**, 8752-8757 (2012).

41 Xu, Y. *et al.* The TRPM1 channel in ON-bipolar cells is gated by both the α and the βγ subunits of the G-protein Go. *Sci Rep* **6**, 20940 (2016).

42 De Silva, S. *et al.* Long-term restoration of visual function in end-stage retinal degeneration using subretinal human melanopsin gene therapy. *Proc Natl Acad Sci U S A* **114**, 11211-11216 (2017).

43 Tsukamoto, H. & Terakita, A. Diversity and functional properties of bistable pigments. *Photochem Photobiol Sci* **9**, 1435-1443 (2010).

44 Koyanagi, M. & Terakita, A. Diversity of animal opsin-based pigments and their optogenetic potential. *Biochim Biophys Acta* **1837**, 710-716 (2014).

45 Strettoi, E. & Pignatelli, V. Modifications of retinal neurons in a mouse model of retinitis pigmentosa. *Proc Natl Acad Sci USA* **97**, 11020-11025 (2000).

46 Gayet-Primo, J. & Puthussery, T. Alterations in Kainate Receptor and TRPM1 Localization in Bipolar Cells after Retinal Photoreceptor Degeneration. *Front Cell Neurosci* **9**, 486 (2015).

47 Gilhooley, M. J. *et al*. ON-bipolar cell gene expression during retinal degeneration: Implications for optogenetic visual restoration. *Experimental Eye Research* **207**, 108553 (2021).

48 Lagali, P. S. *et al.* Light-activated channels targeted to ON bipolar cells restore visual function in retinal degeneration. *Nat Neurosci* **11**, 667-675 (2008).

49 Umino, Y., Solessio, E. & Barlow, R. B. Speed, spatial, and temporal tuning of rod and cone vision in mouse. *J Neurosci* **28**, 189-198 (2008).

50 Benkner, B., Mutter, M., Ecke, G. & Münch, T. A. Characterizing visual performance in mice: an objective and automated system based on the optokinetic reflex. *Behavioral neuroscience* **127**, 788-796 (2013).

Figures

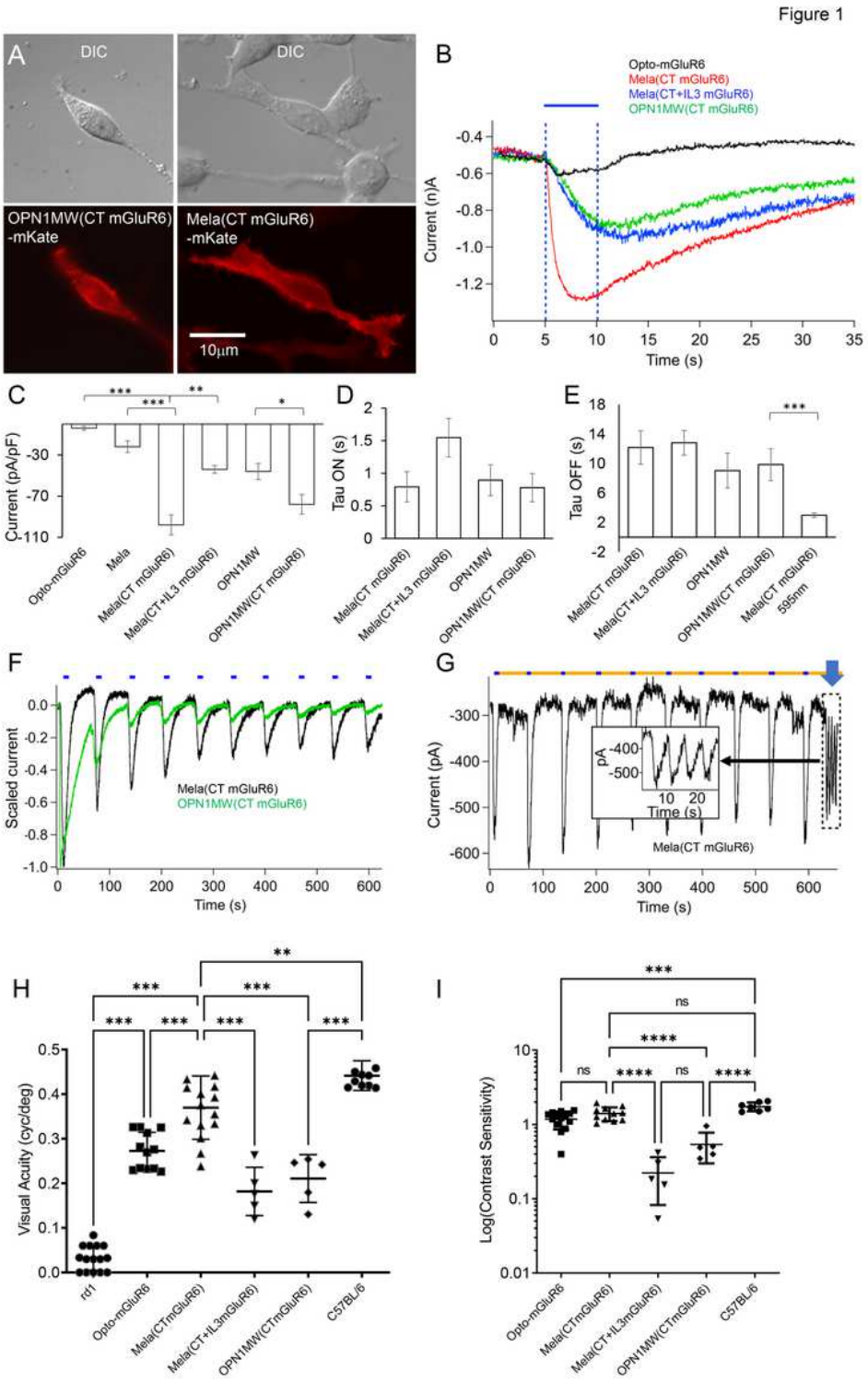

Figure 1

In vitro and in vivo screening of opsin constructs. (A) HEK293-GIRK cells transiently transfected with different Opsin-mKate fusion proteins show robust membrane expression (exemplified for OPN1MW(CT mGluR6)- mKate and Mela(CTmGluR6)-mKate). (B-H) To assess the relative efficacies at

which opsin constructs activate G- proteins in the Gαi/o class, we screened all opsin constructs in HEK293-GIRK cells. (B) Example light responses recorded in HEK293-GIRK cells (stimulus presented by blue bar; 470nm; 1014 photons/cm2/s). (C) Average normalized GIRK response amplitudes recorded under the same conditions as in B. Substituting the C-terminus with that of mGluR6 resulted in significantly larger GIRK responses to light in melanopsin (p=0.0008) and OPN1MW (p=0.0159). (D&E) The relative Tau ON (D) and Tau OFF (E) values of the different opsins in HEK293-GIRK cells using similar data to that presented in B. Although not significant, we observed a slight tendency towards shorter Tau ON values in constructs that generated larger response amplitudes (D). Tau OFF values did not differ significantly, with the exception of 11 of 15 melanopsin chimeras recorded with an orange backlight (E; 595nm at 5 x 1015 photons/cm2/s; p = 0.0008). (F&G) Repetitive light stimuli (5 sec duration at 1min intervals; 470nm; 5 x 1013 photons/cm2/s) in GIRK cells transfected with OPN1MW(CTmGluR6) (F; green) and Mela(CTmGluR6) (F&G; black). Since melanopsin is tri-stable, we observed no bleach run-down when using an orange backlight (G; 595nm at 5 x 1015 photons/cm2/s). This response showed little attenuation, even at 0.2 Hz stimulation (blue arrow; insert). (H & I) In vivo screening of treated blind (>24 weeks) rd1 mice in a naïve optomoter reflex task. (H) Visual acuity thresholds: all opsins restore visual acuity significantly in blind rd1 mice, with Mela(CTmGluR6) significantly outperforming the other constructs [n(rd1) = 15 (negative blind control),

n(rd1_Opto-mGluR6) = 12, n(rd1_Mela-mGluR6(CT) = 16, n(Mela-mGluR6(CT+IL3) = 5, n(OPN1MWW-mGluR6(CT) = 5, n(C57BL/6) = 10 (positive seeing control)]. (I) Contrast Sensitivity thresholds: Mela(CTmGluR6) and Opto-mGluR6 significantly outperform the other constructs, with average contrast sensitivity values for Mela(CTmGluR6) treated mice not being significantly different to those determined in C57BL/6 mice. Since rd1 mice were unable to track at 100% contrast, they are not shown in this graph.

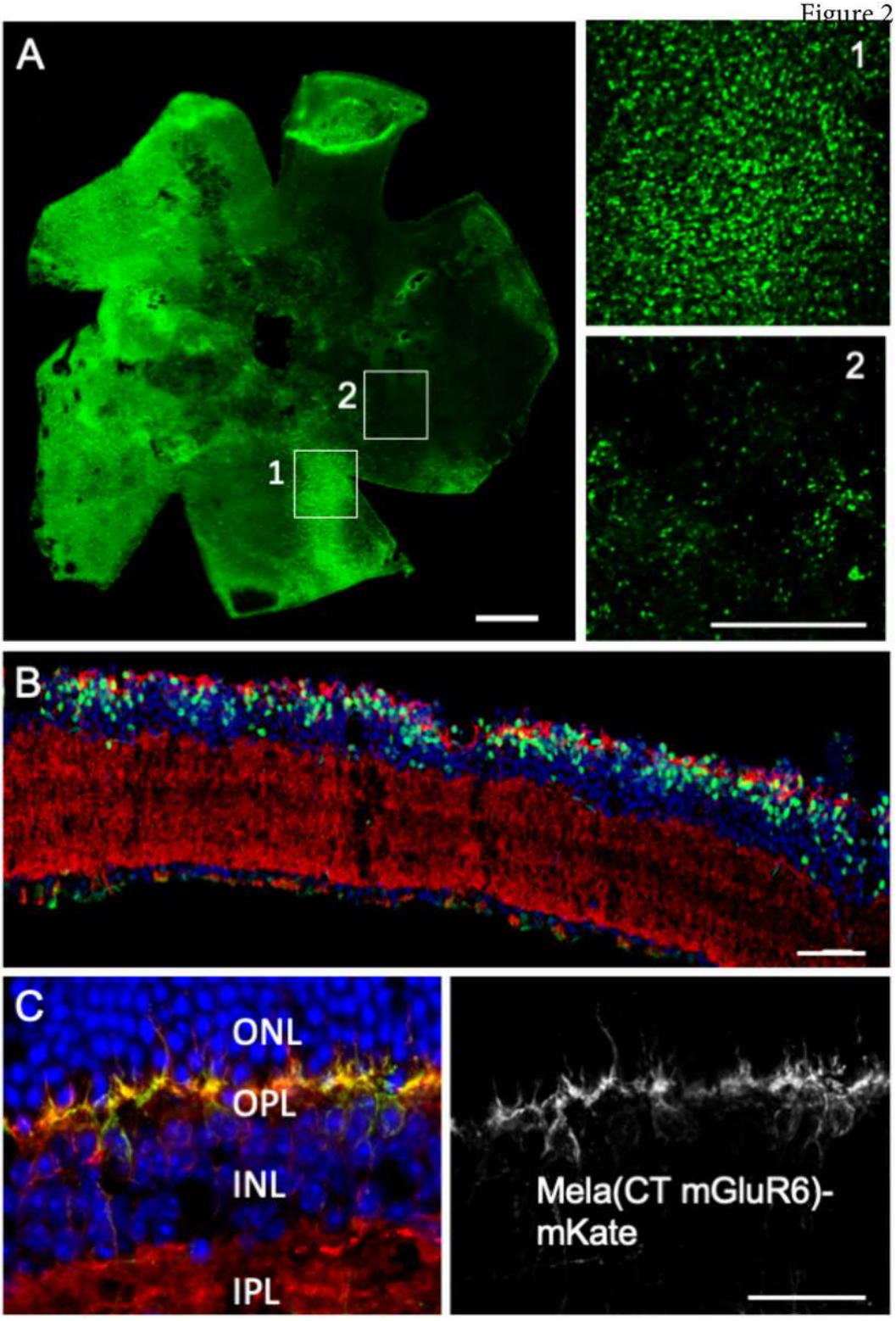

Figure 2

Targeted expression in OBCs after intravitreal injection. (A) A representative rd1 retina four weeks after intravitreal injection of Mela(CTmGluR6)-IRES-TurboFP635. Inserts show higher magnification scanning micrographs

taken from the bipolar cell layer at specified regions, with relatively high (1) or low (2) transduction. Despite the highlighted heterogeneity, OBCs were transduced across the retina. (B) Expression was specific for OBCs in the rd1 retina (TurboFP635 in green; Gαo in red; DAPI in blue). (C) A Mela(CTmGluR6)-mKate fusion protein demonstrates robust targeted expression to the OBC dendrites (mKate in green; Gαo in red; DAPI in blue). Scale bars 500μm in A and 50μm in other panels.

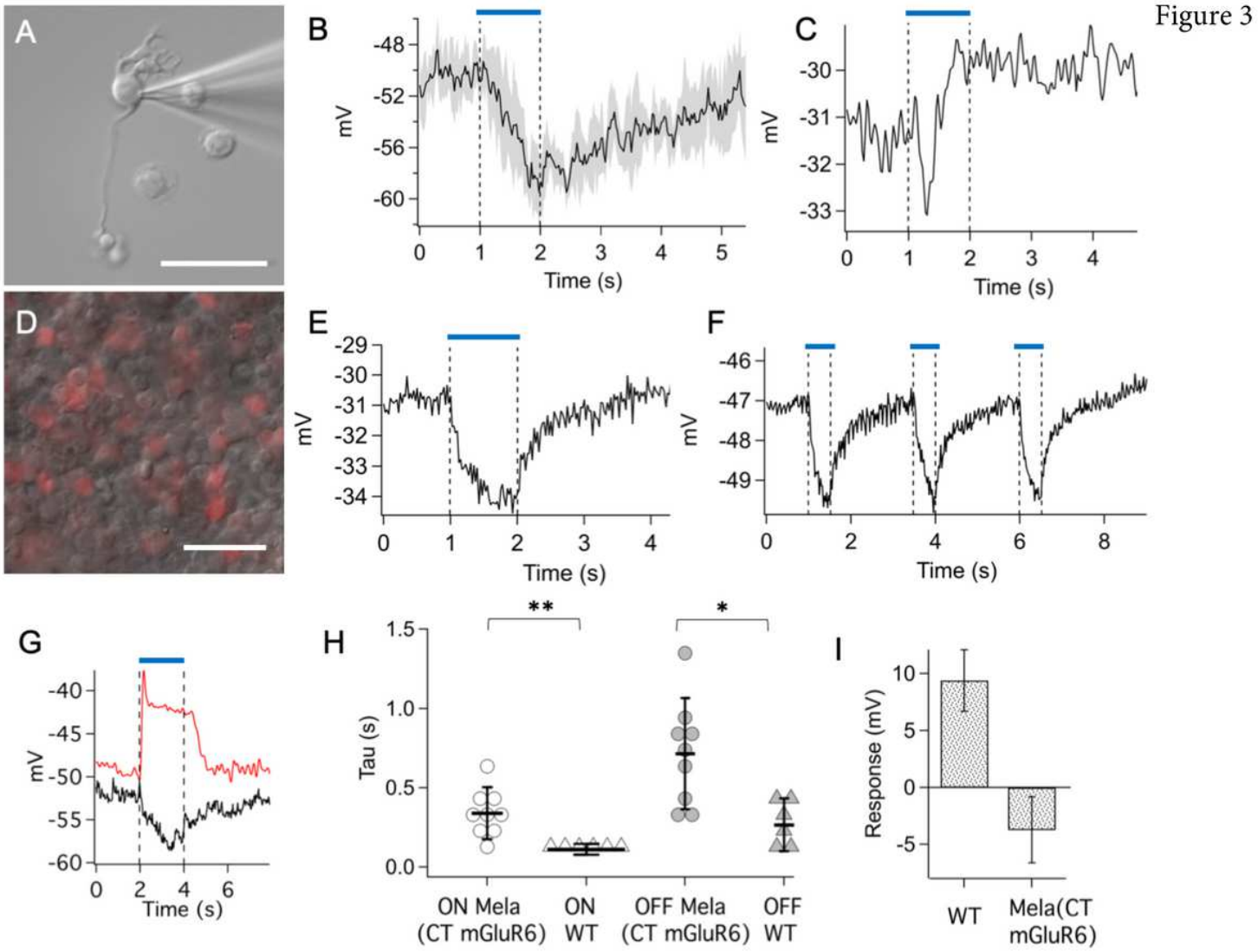

Figure 3

Mela(CTmGluR6) driven light responses in OBCs. (A) We targeted isolated OBCs for electrophysiological recordings by their characteristic morphology under IR-DIC optics and reporter gene expression. (B) Isolated rod bipolar cells responded with a small but consistent hyperpolarization to light (470nm; 1014 photons/cm2/s; trace shows average response of 6 cells with shaded area indicating 1 SD). (C) An isolated cone OBC with a fast, biphasic response to the same light stimulus presented in B demonstrates diverse intrinsic processing within different OBC types. (D) In whole mount rd1 retinas, OBCs were targeted for recording by reporter gene expression and by the characteristic size and location of their cell bodies. (E&F) Recordings from transfected rod bipolar cells in the whole mount rd1 retina had robust light

responses with a faster recovery time compared to isolated cells (E; 470nm; 1013 photons/cm2/s) and could be repeatedly triggered at 0.4 Hz (F). (G) Light responses from a transduced rod bipolar cell in a rd1 whole mount retina (black) compared to a light response form a rod bipolar cells in a wild type C57BL/6 slice preparation of the retina (red; 470nm; 1 x 1013 and 1 x 1011 photons/cm2/s, respectively). (H) Tau ON and Tau OFF values of wild type OBCs (n=6) and Mela(CTmGluR6)-transduced rd1 OBCs (n=9). Although time constants recorded from wildtype cells were on average faster, both, the ON and OFF time constants of some treated cells overlapped with those recorded from wildtype cells ($p = 0.0055$ and 0.0125, respectively). (I) Average response amplitudes of the same responses presented in G. Scale bars in A and D 50 µm

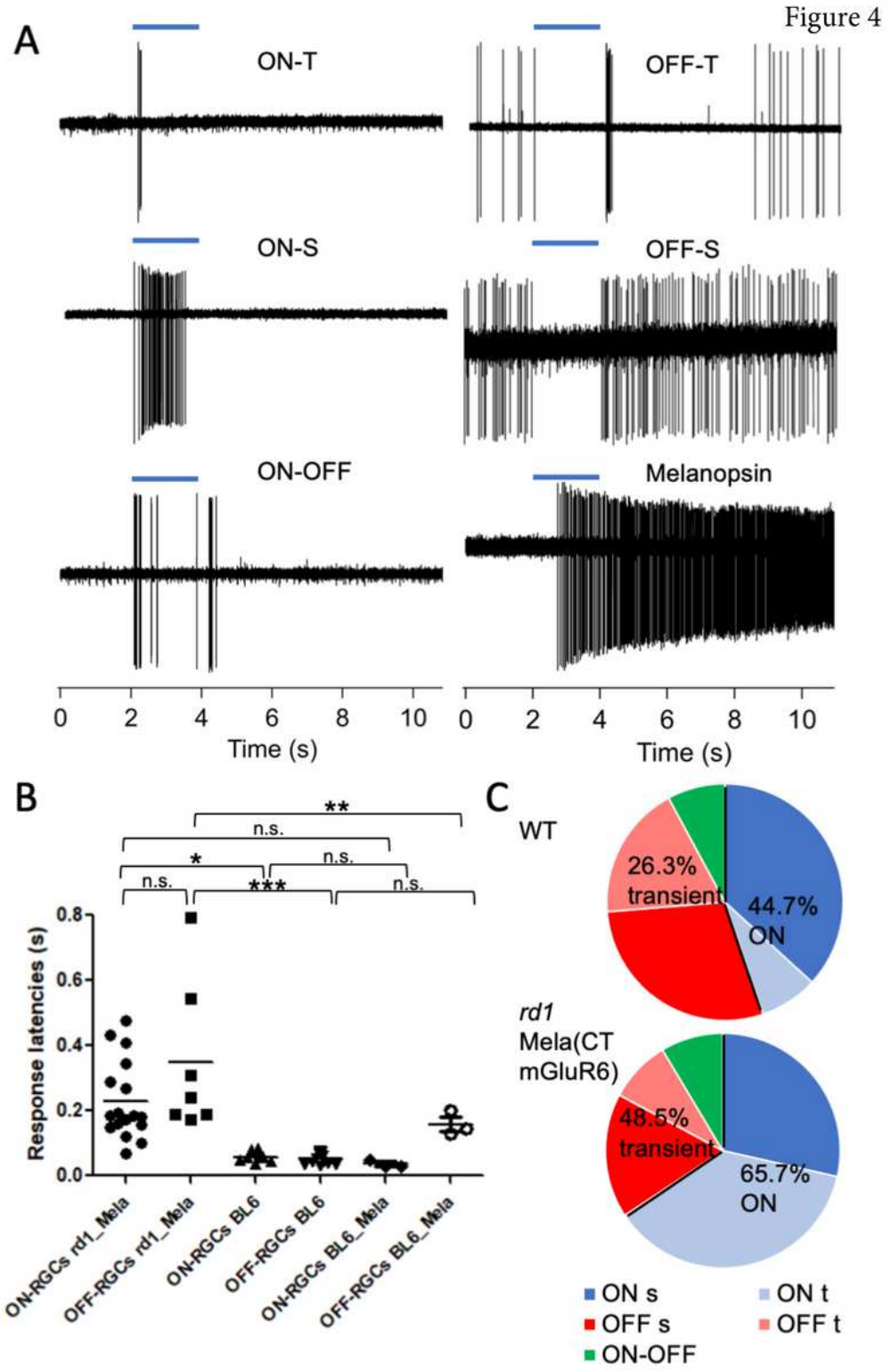

Figure 4

Mela(CTmGluR6) restores diverse receptive-field types in the RGC population of the degenerated rd1 retina. (A) Extracellular recordings from RGCs in the Mela(CTmGluR6)-treated rd1 retina during light stimulation reveal all canonical receptive-field types: transient ON (ON-T), transient OFF (OFF-T), sustained ON (ON-S), sustained OFF (OFF-S), ON-OFF as well as melanopsin responses from ipRGCs. (B) The response onset of ON and OFF RGCs in treated rd1 retinas had a relatively wide scatter compared to

the WT retina. (C) Pie-charts showing the relative fraction of receptive-field types (excluding melanopsin) recorded in the WT and the Mela(CTmGluR6)-treated rd1 retina. Compared to the WT retina, we observed a relative shift from OFF to ON response types and from sustained to transient responses in the treated rd1 retina.

Figure 5

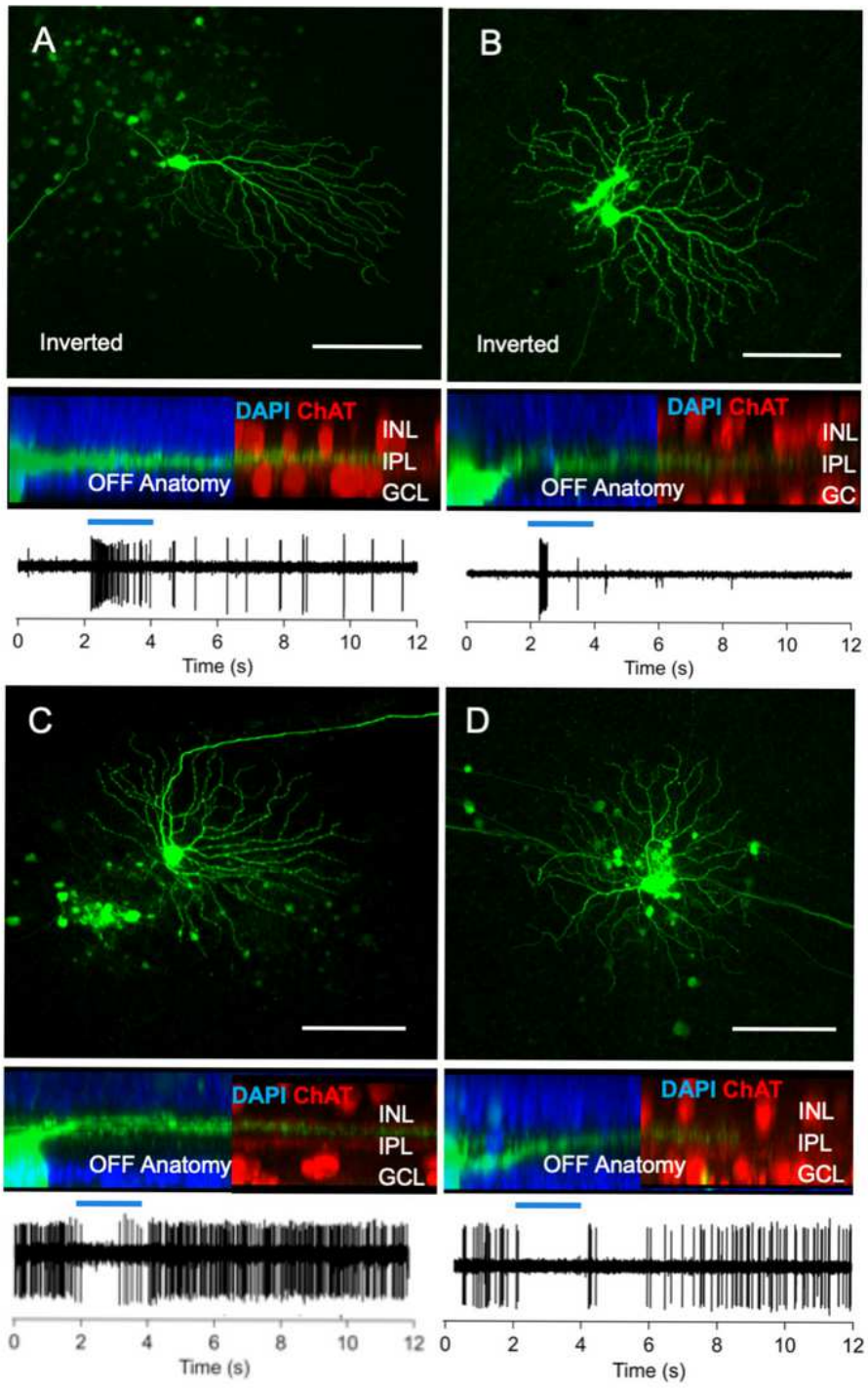

Figure 5

Anatomy-function correlation of Mela(CTmGluR6)-triggered RGC responses in the treated rd1 retina determined by patch-clamp. Anatomy and corresponding light responses of 4 example RGCs from Mela(CTmGluR6)-treated rd1 retinas show that some native OFF RGCs (A&B) have inverted light responses (i.e. dendrites that stratify in the OFF sublamina of the inner plexiform layer (IPL) with a light response at the onset of light), while the light responses of other cells (C&D) are not inverted (i.e. cells that stratify in the OFF sublamina of the IPL respond at the end of the light stimulus). Also see Supplementary Table S2. Light stimulus indicated as blue bar above spike trains (470nm; 1014 photons/cm2/s). Scale bars = 100µm.

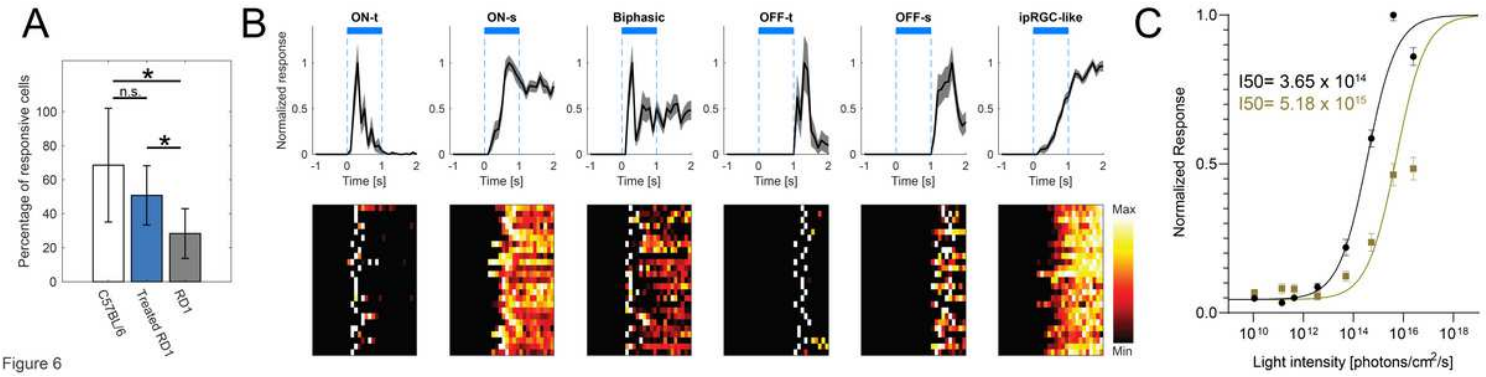

Figure 6

Figure 6

Compound RGC responses in retinas from Mela(CTmGluR6)-treated rd1 mice determined on multi-electrode arrays. (A) We observed a significantly higher percentage of responsive cells in treated rd1 retinas (n=24) compared to untreated rd1 retinas (n=7, p=0.0044). There was no significant difference in percentage of responsive cells between C57BL/6 retinas (n=6) and Mela(CTmGluR6)-treated rd1 retinas (p=0.077). (B) Example average traces of different functional RGC categories. Light stimulation (470nm, 5x1014 photons/cm2/s, 1s) indicated as blue bars. Below each representative average trace (mean ± s.e.m.) is a heat map of representative individual cells. (C) Dark-adapted (black trace) and light-adapted (dark yellow trace) intensity response curves from RGCs of Mela(CTmGluR6)-treated rd1 retinas (n=69 cells). Cells were stimulated every 120s with a blue light flash (470nm, 1.12x1010 – 2.5x1016 photons/cm2/s), light adaptation for 15 minutes (white light at 100 µW cm−2) and then the stimulation protocol was repeated. I50(dark-adapted) = 3.65 x 1014 photons/cm2/s, I50(light-adapted) = 5.18 x 1015photons/cm2/s.

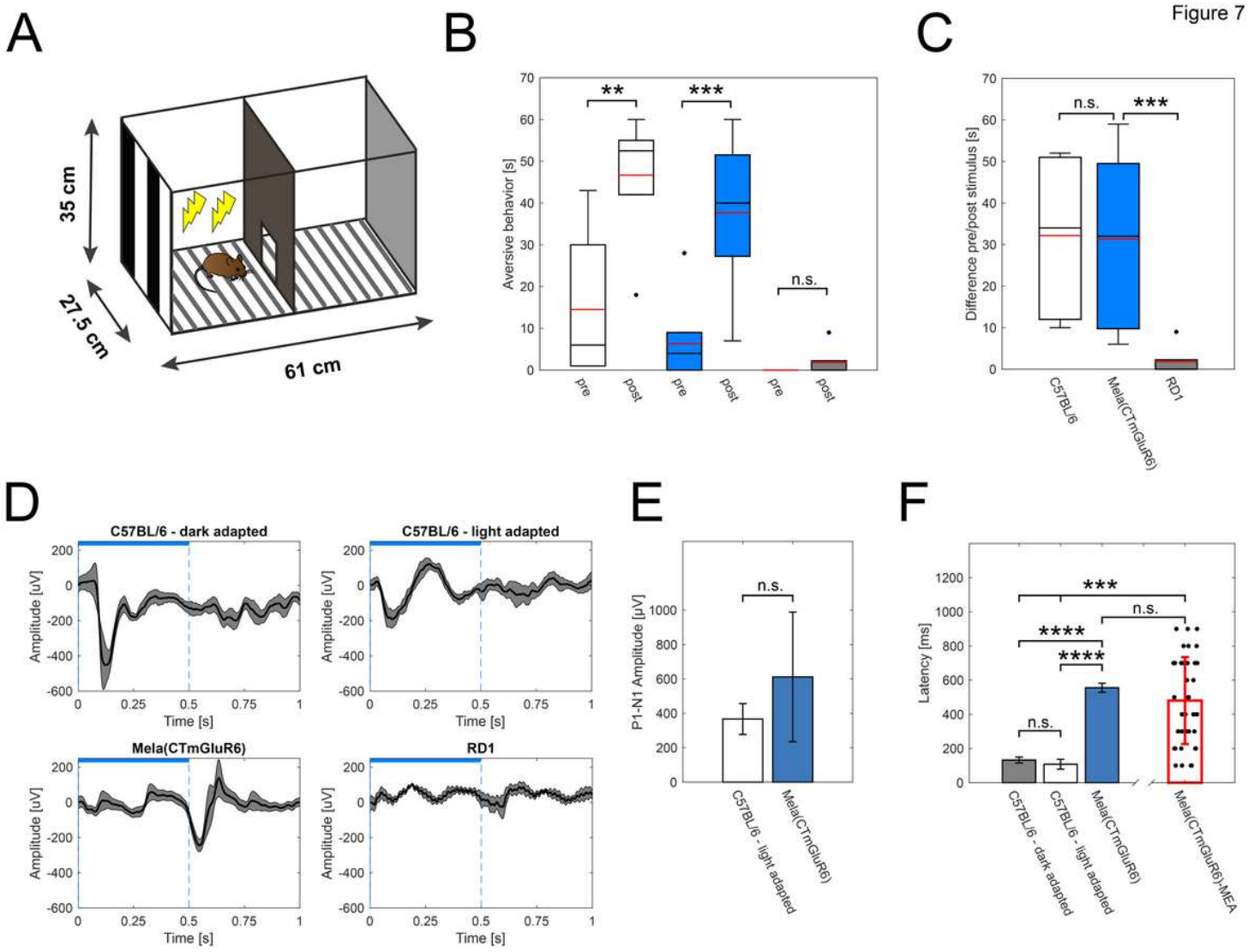

Figure 7

Restoration of conditioned visually guided behavior. (A) Graphical depiction of the two-compartment visual conditioning paradigm to a moving grating (0.35 cyc/deg spatial frequency). (B) Comparison of aversive behaviors on day 4 before and during the pattern display increased significantly in C57BL/6 controls (p=0.00263) and Mela(CTmGluR6)-treated rd1 mice (p=0.00026), while non-treated rd1 mice did not show a behavioral response to the pattern stimulus. Shown are medians ± SD, red vertical lines denote the means. See movie M1 in the supplementary information for a typical behavior of a treated rd1 mouse in response to the drifting gratings. Comparsion of 60 seconds pre-stimulus vs. 60 seconds during stimulus. (C) Stimulus-triggered aversive behavior was equally observed in Mela(CTmGluR6) injected rd1 mice (n=9) and healthy C57BL/6 mice (positive control, n=6; p=0.9935), but not in

untreated rd1 littermates (negative control, n=5; p = 0.00005). (D) Average VEP responses to a full-field light stimulus 13 of 15(470nm, 5 x 1013 photons/cm2/s, 500 ms) in dark-adapted C57BL/6 animals (n=9 traces), light-adapted C57BL/6 animals (n=6 traces), Mela(CTmGluR6)-treated rd1 animals (n=22 traces) and untreated rd1 controls (n=9 traces). (E) Comparison

of P1-N1 amplitudes in light adapted C57BL/6 animals (367 ± 90 µV; n=6 traces) and Mela(CTmGluR6)-treated rd1 animals (612 ± 377 µV; n=22 traces). No significant differences were observed between experimental groups (p=0.043). (F) Comparison of response latencies. The latency was significantly increased in Mela(CTmGluR6) treated rd1 animals (556 ± 27 ms, n=22 traces) in comparison to dark-adapted C57BL/6 mice (132 ± 18 ms, n=9 traces, p<0.000001) and light- adapted C57BL/6 mice (108 ± 29 ms, n=6 traces, p=<0.000001). No significant difference was observed between dark- and light-adapted C57BL/6 animals (p=0.0596). Latencies of light-intensity matched MEA recordings from RGCs of Mela(CTmGluR6) treated rd1 mice (481 ± 254 ms; n=41 cells; 500ms; 470nm; 5x1013 photons/cm2/s) did not differ significantly from the V1 latencies in Mela(CtmGluR6) treated mice (p= 0.173). Dots in MEA recordings represent values of individual cells.

Supplementary Files

This is a list of supplementary files associated with this preprint. Click to download.

- SupplementalMaterialKleinlogel.pdf